WAGNER, Norman Keith, 1932-
A TWO-DIMENSIONAL, TIME DEPENDENT NUMERICAL MODEL OF ATMOSPHERIC BOUNDARY LAYER FLOW OVER INHOMOGENEOUS TERRAIN.

University of Hawaii, Ph.D., 1966
Physics, meteorology

University Microfilms, Inc., Ann Arbor, Michigan

A TWO-DIMENSIONAL, TIME DEPENDENT NUMERICAL MODEL OF ATMOSPHERIC BOUNDARY LAYER FLOW OVER INHOMOGENEOUS TERRAIN

A DISSERTATION SUBMITTED TO THE GRADUATE SCHOOL OF THE

UNIVERSITY OF HAWAII IN PARTIAL FULFILLMENT

OF THE REQUIREMENTS FOR THE DEGREE OF

DOCTOR OF PHILOSOPHY

IN METEOROLOGY

SEPTEMBER 1966

By

Norman Keith Wagner

Dissertation Committee:

Mariano A. Estoque, Chairman
Wan-Cheng Chiu
Colin S. Ramage
Edwin H. Mookini
Walter R. Steiger

ABSTRACT

A two-dimensional, time dependent, numerical model of the atmospheric boundary layer is formulated and used to investigate various characteristics of air motion when a change occurs in the roughness of the underlying surface. The model assumes a dry adiabatic atmosphere and adiabatic changes of state, no dynamic pressure effects due to flow accelerations and no vertical displacement of the zero-velocity level at the lower boundary when a discontinuity in surface roughness is encountered. Numerical evaluation of all terms in the resulting equations shows little change in the computed fields of velocity if an incompressible atmosphere is assumed and horizontal mixing is neglected.

A computational stability analysis is made which provides the relationship between time-step and grid spacing necessary to insure convergence of the numerical solution. For horizontally homogeneous conditions, comparison of the numerical solutions with various analytical solutions shows that the errors inherent in the finite difference formulation can be reduced to any desirable level by reducing the grid spacing, particularly near the lower boundary.

Computed quantities include the two-dimensional distributions of horizontal velocity, vertical velocity and eddy shearing stress. Increasing surface roughness causes a decrease in the horizontal velocity near the lower boundary. This results in upward vertical motion. For a prevailing geostrophic wind speed of 10 m/sec and roughness parameters varying from 1 cm through 10 cm, maximum vertical motion on the order of 5 cm/sec is found over the roughness

discontinuity at heights ranging from 50 to 100 meters. Vertical velocities in excess of 0.1 cm/sec are found several meters upstream from the discontinuity and persist for several hundred meters downstream for the cases considered.

The computations also show that a nearly logarithmic wind profile with associated constant shearing stress becomes established throughout a layer which increases in depth with distance downwind from the roughness discontinuity. The ratio of depth to downwind distance of this layer lies between 1/50 and 1/100. Reestablishment of the logarithmic profile does not imply equilibrium flow, however. It is found that a fetch on the order of several kilometers is necessary before the surface eddy stress differs by less than ten percent from the final equilibrium values.

Excellent quantitative agreement is found with Panofsky and Townsend (1964), who employed data of Kutzbach (1961) to show that their theory agreed with observations. Because of the inability of the numerical model to consider zero-plane displacement and non-neutral atmospheric stability, both of which are probably significant and certainly present in the observations available from the University of Wisconsin, no further quantitative comparisons were made. However, the general features of the computed velocity and stress distributions agree very well with results of Stearns and Lettau (1963), hence there is at least good qualitative agreement with observations.

Suggestions are made for generalizing and improving the numerical model.

TABLE OF CONTENTS

LIST OF TABLES

LIST OF FIGURES

I. INTRODUCTION

At elevations well above the disturbing effects of the earth's surface, the main forces which influence atmospheric motion are the pressure, centrifugal and coriolis forces. The pressure force is real and has its genesis in the non-uniform absorption and emission of radiation by the earth-atmosphere system, while the centrifugal and coriolis forces are apparent forces arising from the curvature of the flow and the rotation of the earth, respectively. When the mean flow is steady, straight and horizontal, the horizontal components of the pressure force and the coriolis force are in balance. This balance of forces is referred to as the geostrophic balance, and the associated wind is the geostrophic wind. It is significant that in non-tropical latitudes, the free atmosphere frequently approaches a state of geostrophic balance.

Eliminating vertical perturbations of the type which might arise from thermal convection, one would expect geostrophic balance to be achieved when the magnitude of the surface induced frictional force becomes negligibly small compared to the other forces which affect the air motion. Under conditions of horizontally homogeneous terrain and neutral atmospheric stability (i.e., constant potential temperature), most theoretical studies (Taylor (1915), Köhler (1933), Ellison (1956), Lettau (1962), Blackadar (1962)) place the height at which the surface induced frictional force becomes negligible near 1000 meters. The layer of air in which surface frictional effects are significant has been called the "planetary boundary layer" by Lettau (1939). Other terms commonly used to describe this layer are "atmospheric boundary layer" and "friction layer".

From these theoretical studies one finds that the height of this boundary layer increases with increased surface friction, however, only a small change in height is found for quite large variations in surface roughness and prevailing wind speed (Blackadar (1962)). Although far from conclusive, there is some observational evidence to support this theoretical result (Dobson (1914), Mildner (1932), Lettau (1950), Lettau and Davidson (1957), Holzworth (1964)).

All of the theoretical studies previously mentioned assume that the flow is one dimensional; that is, steady state, horizontally uniform flow over horizontally homogeneous terrain. Once the functional form of the frictional force is specified, along with upper and lower boundary conditions, it is possible to derive the height variation of the horizontal wind. Boundary conditions usually require the wind speed to be zero at the earth's surface and approach the geostrophic value at high elevations. Two of the more recent specifications of the frictional force are those of Blackadar (1962) which is based on a non-dimensional examination of existing atmospheric data under neutral atmospheric stability, and Lettau (1961, 1962), which combines atmospheric and duct flow data. Both developments yield essentially the same results.

Once the structure of the wind has been determined near the earth's surface, it is possible to compute the shearing stress, and hence, the flux of momentum between the earth and the atmosphere. This has been done for the entire northern hemisphere by Kung (1963) using Lettau's boundary layer model. Kung empirically specified a surface roughness parameter based on land use statistics at 360 locations and computed the mean energy dissipation in the planetary boundary layer at these locations by utilizing daily surface pressure patterns for a ten-year period. Estimates of frictional dissipation of energy have also been made over the British Isles for a three-month period by Holopainen (1964) and over North America for a six-month period by Kung (1966) by employing energy balance techniques. Frictional dissipation of air flow over a forest has been investigated by Johnson (1965).

One of the reasons for the current interest in the mechanisms of energy transfer in the atmosphere is related to the problems of long range weather forecasting. By estimating the mean reservoir of atmospheric mechanical energy and the global mean of energy dissipation, Lettau (1959) has shown that there is a renewal period for kinetic energy of about three days. This would suggest that any prediction scheme for periods greater than one or two days must include a specification of the momentum flux due to frictional dissipation (Holopainen (1963)). A fairly precise knowledge of both the spacial and temporal variations of the momentum flux would seem necessary before accurate forecasts are possible for periods in excess of a week.

Variations in space and time of the flux of mass, momentum, and heat are also of importance in many studies involving local, or relatively small scale circulations. This problem is rarely more than just mentioned in textbooks on boundary layer theory, that by Laikhtman (1961) being a notable exception. Increased knowledge of the physical and dynamical effect of horizontal inhomogeneities in surface terrain is needed so that we might more accurately model various atmospheric phenomena. For example, dynamical models of the sea breeze (Estoque (1962)), mountain-valley winds (Orville (1964)), air mass transformation (Asai (1965)), and wind drift of ice floes (Laikhtman (1961)), are but a few instances where the effects of spacial variations in the lower boundary conditions must play a significant role in the resulting motions and energy transformations.

Attempts have been made to examine the variation in momentum flux due to spacial variations in surface roughness characteristics by Elliott (1958), Taylor (1962), and Panofsky and Townsend (1964). Although these studies were motivated primarily to determine the representativeness of vertical gradient measurements taken over sites of limited horizontal extent, the results, are, nevertheless, just as pertinent in their application to the problems of the atmospheric energy balance and local circulations. All three of these studies have concentrated on the downwind variation of the momentum flux in a neutral atmosphere when an abrupt change occurs in z_0, a parameter which characterizes the surface roughness. The problem is treated as steady state, and particular attention is focused on the development and downwind change in height of an internal boundary layer. This internal boundary layer (or zone) separates flow which is in equilibrium with the upwind surface from that which is approaching equilibrium with the downwind surface.

The assumption basic to Elliott's development is that the internal boundary layer is a surface which separates two equilibrium flows. Velocity is continuous at the interface, but the shearing stress is necessarily discontinuous in his model. Panofsky and Townsend generalize Elliott's model to allow for stress (through the friction velocity) to vary continuously with height. In this way, both velocity and stress can be made continuous at the interface, an arrangement which appears physically more realistic. In this case, the interface becomes a zone of transition separating flow above, which has not "felt" the new surface, from flow below, which is nearly in equilibrium with the new surface roughness. Both Elliott, and Panofsky and Townsend predict large overcompensation of the surface shearing stress when an abrupt change in roughness is encountered, followed by gradual approach to the new equilibrium value.

Taylor, on the other hand, uses wind tunnel observations of Jacobs (1939) to argue that the leading edge of the transition zone is nearly vertical and that the new surface stress is attained after a relatively short fetch. Panofsky and Townsend, however, have pointed out the scaling difficulties inherent in attempting to relate wind tunnel observations to atmospheric phenomena. In addition, they show that data presented by Taylor in support of his model are not definitive, but can be used equally well in support of Elliott's or their own model.

Observational programs at the University of Wisconsin by Kutzbach (1961), Stearns and Lettau (1963) and Stearns (1964) appear to support the results of Panofsky and Townsend. Kutzbach used an array of inverted bushel baskets placed on a smooth frozen lake, while Stearns employed Christmas trees on the frozen lake as the device for changing the surface roughness characteristics. Comparison with predicted and observed wind profiles is shown to be quite good for flow over the bushel baskets (Panofsky and Townsend (1964)). The analysis by Stearns and Lettau of the momentum budget in the vicinity of the roughness discontinuity is at least in qualitative agreement with the prediction of Panofsky and Townsend.

The present development will attack the problem of air flow over inhomogeneous terrain in a somewhat different and considerably more general way than any of the preceding works. We shall retain time as an independent variable and permit the occurrence of both local and advective changes in the velocity field. Because the roughness change represents a horizontal discontinuity, we shall also retain those terms in the basic physical equations which relate to horizontal mixing. The assumption basic to our model is that the mixing length (defined and described in Chapter II) changes abruptly, simultaneously with the change in roughness. When this assumption is incorporated into the equations of motion and the equation of continuity, then the horizontal and vertical fields of velocity, and the associated momentum flux may be derived. Because of the non-linear nature of the resulting partial differential equations, we shall formulate finite-difference analogues to these equations and solve the finite-difference equations by numerical techniques.

II. MATHEMATICAL DEVELOPMENT

If we confine ourselves to non-relativistic (Newtonian) mechanics and assume no mass-energy conversions, the mathematical statements of the basic physical conservation principles consist of Newton's laws of motion, the equation of mass continuity and the first law of thermodynamics. We shall assume that the atmosphere behaves as an ideal gas and that the only real forces acting on the air are pressure, friction, and gravity. Since horizontal dimensions to be considered are on the order of a few kilometers, the earth may be assumed to be flat. In addition, we shall assume molecular viscosity to be negligible compared with eddy viscosity (Sutton (1953)). The equations of motion on the rotating earth for mean flow may then be written in component form: (see Appendix for definitions of symbols)

$$(2.1)\quad \frac{du}{dt} = 2\Omega v \sin(lat) - 2\Omega w \cos(lat) + \frac{1}{\rho}\left[\frac{\partial \tau_{xx}}{\partial x} + \frac{\partial \tau_{xy}}{\partial y} + \frac{\partial \tau_{xz}}{\partial z} - \frac{\partial p}{\partial x}\right]$$

$$(2.2)\quad \frac{dv}{dt} = -2\Omega u \sin(lat) + \frac{1}{\rho}\left[\frac{\partial \tau_{yx}}{\partial x} + \frac{\partial \tau_{yy}}{\partial y} + \frac{\partial \tau_{yz}}{\partial z} - \frac{\partial p}{\partial y}\right]$$

$$(2.3)\quad \frac{dw}{dt} = -2\Omega u \cos(lat) - g + \frac{1}{\rho}\left[\frac{\partial \tau_{zx}}{\partial x} + \frac{\partial \tau_{zy}}{\partial y} + \frac{\partial \tau_{zz}}{\partial z} - \frac{\partial p}{\partial z}\right]$$

The equation of continuity may be written:

$$(2.4)\quad -\frac{1}{\rho}\frac{d\rho}{dt} = \frac{\partial u}{\partial x} + \frac{\partial v}{\partial y} + \frac{\partial w}{\partial z}$$

and the first law of thermodynamics as:

$$\text{(2.5)} \qquad \frac{dq}{dt} = c_p \frac{dT}{dt} - \frac{1}{\rho} \cdot \frac{dp}{dt}$$

where

$$\text{(2.6)} \qquad p = \rho R T$$

is the equation of state for an ideal gas.

The vertical motion contribution through the coriolis term on the right side of equation (2.1) is generally negligible. If we let $f = 2\Omega \cdot \sin$ (lat) and write the horizontal pressure force in terms of geostrophic wind components, we have:

$$\text{(2.7)} \qquad \frac{du}{dt} = f(v - v_g) + \frac{1}{\rho}\left[\frac{\partial \tau_{xx}}{\partial x} + \frac{\partial \tau_{xy}}{\partial y} + \frac{\partial \tau_{xz}}{\partial z}\right]$$

$$\text{(2.8)} \qquad \frac{dv}{dt} = f(u_g - u) + \frac{1}{\rho}\left[\frac{\partial \tau_{yx}}{\partial x} + \frac{\partial \tau_{yy}}{\partial y} + \frac{\partial \tau_{yz}}{\partial z}\right]$$

Assuming further that only adiabatic changes of state occur and that the dependent variables u, v, and τ are not functions of y we have equations (2.7), (2.8), (2.4), (2.5) as:

$$\text{(2.9)} \qquad \frac{\partial u}{\partial t} + u\frac{\partial u}{\partial x} + w\frac{\partial u}{\partial z} = f(v - v_g) + \frac{1}{\rho}\left[\frac{\partial \tau_{xx}}{\partial x} + \frac{\partial \tau_{xz}}{\partial z}\right]$$

$$(2.10)\quad \frac{\partial v}{\partial t} + u\frac{\partial v}{\partial x} + w\frac{\partial v}{\partial z} = f(u_g - u) + \frac{1}{\rho}\left(\frac{\partial \tau_{yx}}{\partial x} + \frac{\partial \tau_{yz}}{\partial z}\right)$$

$$(2.11)\quad -\frac{1}{\rho}\frac{d\rho}{dt} = \frac{\partial u}{\partial x} + \frac{\partial w}{\partial z}$$

$$(2.12)\quad 0 = c_p\frac{dT}{dt} - \frac{1}{\rho}\frac{dp}{dt}$$

When the inertial terms of equation (2.3) are assumed to vanish, we obtain the hydrostatic equation:

$$(2.13)\quad \frac{\partial p}{\partial z} = -\rho g$$

Although these inertial terms are not identically zero in our development, they are, nevertheless, several orders of magnitude smaller than the hydrostatic terms. We shall assume (2.13) to be an adequate representation of (2.3). Once the functional form of the frictional stresses τ_{12} is specified, equations (2.6) and (2.9) through (2.13) form a set of six equations in the six dependent variables u, v, w, p, ρ, and T and three independent variables x, z, and t.

We may combine equations (2.6), (2.11), (2.12), and (2.13) to obtain an explicit equation for vertical velocity w. Elimination of temperature from (2.6) and (2.12) gives the adiabatic relationship between pressure and density:

$$(2.14) \qquad \frac{(1-\kappa)}{p} \cdot \frac{\partial p}{\partial t} = \frac{1}{\rho} \cdot \frac{\partial \rho}{\partial t}$$

where $R/c_p = \kappa$.

Substitution of (2.14) into (2.11) gives, upon expansion of the total derivative:

$$(2.15) \qquad \frac{(1-\kappa)}{p}\left[\frac{\partial p}{\partial t} + u\frac{\partial p}{\partial x} + v\frac{\partial p}{\partial y} + w\frac{\partial p}{\partial z}\right] + \frac{\partial u}{\partial x} + \frac{\partial w}{\partial z} = 0$$

Differentiating equation (2.15) with respect to z , substituting the geostrophic wind relationships for the horizontal pressure gradients and assuming hydrostatic equilibrium yields

$$(2.16) \qquad \frac{\partial^2 w}{\partial z^2} - \frac{\rho g}{p}\cdot\frac{\partial w}{\partial z} = \frac{\kappa g \rho}{p}\cdot\frac{\partial u}{\partial x} - \frac{\partial^2 u}{\partial z \partial x} + \frac{\rho(1-\kappa)f}{p}\cdot\left(u_g\frac{\partial v}{\partial z} - v_g\frac{\partial u}{\partial z}\right)$$

which is the desired equation for vertical velocity. It should be noted that equation (2.16) is a diagnostic equation (time independent) as compared to the prognostic form of equations (2.9) and (2.10) for u and v .

If we now assume an environment with a dry adiabatic temperature stratification, the thermodynamic variables are restricted such that once the horizontal pressure gradient (i.e., geostrophic wind), potential temperature, and pressure at any single height are specified, the spacial distributions of density, pressure, and temperature are completely specified. The percentage variation in the magnitude of density, pressure or temperature is relatively small over the entire surface of the earth, hence, a single set of representative values as a function of height should suffice as far as the solution of our system of equations is concerned. Spacial and temporal variations in the horizontal pressure gradient do occur, however. One could investigate the effect of these variations by appropriate specification of the geostrophic wind. Thus, our system of equations reduces to (essentially) the three equations (2.9), (2.10), and (2.16) in three dependent variables u, v, and w and three independent variables x, z, and t.

The precise form of the wind distribution, however, cannot be determined until some hypothesis concerning the distribution of frictional (Reynold's) stress is introduced. According to Sutton (1951), attempts at formulating such a hypothesis began in 1877 with Boussinesq who adopted the fundamental ideas of the kinetic theory of gases by expressing a virtual coefficient of eddy viscosity defined in much the same way as the molecular counterpart. These quantities were called "Austausch" (exchange) coefficients by Schmidt in an extensive monograph on atmospheric boundary layer turbulence published in 1925. In laminar flow the shearing stress is $\mu = (\partial u/\partial z)$ where μ is the dynamic viscosity of the fluid. By analogy, the Reynold's stress may be written:

$$\tau_{xz} = -\rho\overline{u'w'} = A'_z \frac{\partial u}{\partial z} = K_z \rho \frac{\partial u}{\partial z}$$

The quantity A_z' is the exchange coefficient and corresponds to the dynamic viscosity while the quantity K_z is called the eddy viscosity (or eddy diffusivity) and corresponds to the kinematic viscosity. We may also write:

$$\tau_{xx} = K_x \rho \frac{\partial u}{\partial x}$$

$$\tau_{yx} = K_x \rho \frac{\partial v}{\partial x}$$

$$\tau_{yz} = K_z \rho \frac{\partial v}{\partial z}$$

and substitution into (2.9) and (2.10) gives:

$$(2.17) \quad \frac{\partial u}{\partial t} + u\frac{\partial u}{\partial x} + w\frac{\partial u}{\partial z} = f(v - v_g) + \frac{\partial}{\partial x}\left(K_x \frac{\partial u}{\partial x}\right) + \frac{\partial}{\partial z}\left(K_z \frac{\partial u}{\partial z}\right)$$

$$(2.18) \quad \frac{\partial v}{\partial t} + u\frac{\partial v}{\partial x} + w\frac{\partial v}{\partial z} = f(u_g - u) + \frac{\partial}{\partial x}\left(K_x \frac{\partial v}{\partial x}\right) + \frac{\partial}{\partial z}\left(K_z \frac{\partial v}{\partial z}\right)$$

The relationship between the horizontal and vertical eddy diffusivities is rather uncertain. A first approximation frequently made in meteorology is that $K_x = K_z$. Examination of observational data (Yamamoto and Shimanuki (1964)) suggests that the ratio of the cross-wind to the vertical diffusivity under neutral conditions is approximately 13. It has not been established, however, that this same ratio would be appropriate for the downwind diffusivity, K_X . At this point in our development, we shall not make any restricting assumption concerning the relationship between K_X and K_Z . Instead, the effect on the mean flow of various K_X/K_Z ratios will be examined in Chapter VII.

It was quickly and widely recognized that, unlike the molecular viscosity, the eddy viscosity is not a fluid constant. Instead, it appeared to be not only a function of height, but also of the underlying surface roughness. In an attempt to improve the treatment without entirely abandoning the molecular theory analogy, Prandtl (1935) introduced the mixing-length hypothesis. The mixing-length ℓ characterizes the local intensity of turbulent mixing at a given point in the fluid and is analogous to the "mean free path" of kinetic theory. Unlike the "mean free path", however, the mixing length may be a function of position, mean velocity or other fluid parameters.

Using this mixing-length concept it is possible to show (Sutton (1953), p. 73) that the eddy viscosity may be written as the product of the square of the mixing-length times the magnitude of the vertical shear of the mean horizontal wind. In our notation this appears as:

$$(2.19) \qquad K_z = \ell^2 \left[\left(\frac{\partial u}{\partial z} \right)^2 + \left(\frac{\partial v}{\partial z} \right)^2 \right]^{1/2}$$

According to Sutton (1951), "The advantages to be gained by such dissections are not immediately obvious, since the analysis gives no clue to possible variations of ℓ with any of the variables. In practice, the introduction of the mixing-length has proved very useful, since it has been found that only very simple assumptions regarding ℓ are required to obtain a satisfactory mathematical representation of many complex phenomena."

One such attempt, by Rossby and Montgomery (1935), assumes a two layer atmosphere where $\ell = k\,(z + z_0)$ in the lower layer. If the shearing stress is supposed invariable with height through this layer, then the assumed distribution of ℓ gives the familiar logarithmic wind profile

$$(u^2 + v^2)^{1/2} = \frac{V_*}{k} \ln \frac{z + z_0}{z_0}$$

where $V_* \equiv \sqrt{\tau_0 / \rho}$ is called the friction velocity. This profile is now widely accepted as adequately describing the mean wind distribution in the lower layers of the atmosphere under steady state conditions, neutral stability and horizontal homogeneity (Lumley and Panofsky (1964), Priestley (1959), Sutton (1953)). In the upper layer, Rossby and Montgomery assumed ℓ proportional to (H' - Z) where H' is the top of the friction layer.

One disadvantage of the preceding approach is the necessity to select, rather arbitrarily, where one stops using one expression for ℓ and begins to use the other. It would obviously be desirable to have a single expression for the mixing-length which could be applied throughout the entire atmospheric boundary layer. Two such expressions have been derived by Lettau (1961, 1962) and Blackadar (1962).

Lettau obtains his result by considering the analogous flow patterns between duct and atmospheric boundary layer flow. After non-dimensionalizing the governing equations, an expression for the characteristic length scale of turbulence (mixing-length) is obtained which is a function of distance from the boundary and the type of flow (i.e., whether duct or atmospheric flow). For atmospheric flow, Lettau's expression is:

$$\ell = k(z + z_0) \Big/ \left[1 + 4\left(\frac{z + z_0}{H}\right)^{5/4} \right]$$

where H is defined as the "scale height of the boundary layer". The quantity H is not prescribed but is a function of the flow conditions and must be obtained by integration of the equations of motion. To do this, Lettau (1962) notes that a level of maximum eddy viscosity must exist in the boundary layer, and hypothesizes that this level: (a) occurs at one-half the "scale-height", and (b) coincides with the level of maximum cross-isobar flow.

Blackadar, on the other hand, employs physical intuition to argue that ℓ must change from the value as used by Rossby and Montgomery near the earth's surface, to a nearly constant value at higher elevations. He assumes a form for ℓ as given by:

(2.20) $$\ell = k(z + z_0) \Big/ \left[1 + k(z + z_0)/\lambda \right]$$

where λ represents the limiting value for ℓ at high elevation. By using dimensional analysis techniques and available observational data, he obtains the expression:

(2.21) $$\lambda = 0.00027\,(u_g^2 + v_g^2)^{1/2} \big/ f$$

Although their fundamental approach is quite different, the final results of both Blackadar and Lettau for atmospheric boundary layer flow are very similar. Both have the mixing-length increasing linearly with height near the earth's surface and approaching a constant, or nearly constant, value at higher levels. Observational evidence is not sufficiently precise to show unequivocal preference of one over the other. In the computations to be presented in later sections of this paper, we shall use Blackadar's expression.

The system of equations which will be solved consists of (2.16), (2.17), and (2.18) with K_z given by (2.19), ℓ given by (2.20) along with (2.21) and K_x equal to some multiple of K_z. Once the large scale features of the flow and the surface roughness have been specified; that is, the latitude (giving f), the geostrophic wind components, and the distribution of z_0, then equations (2.16), (2.17), and (2.18) may be solved for the velocities u, v, and w.

III. FINITE DIFFERENCE EQUATIONS AND BOUNDARY CONDITIONS

Analytic solutions to equations (2.16) through (2.21) can be obtained in only a limited number of special, simplified cases. The complete equations are most easily "solved" by replacing these non-linear, second order partial differential equations with an equivalent set of linear, algebraic finite-difference equations. Our primary interest lies in examining the details of the velocity distribution near a discontinuity in surface roughness. Since, for computational economy, we wish to keep the total number of grid points as small as possible, it seems logical to choose a finite-difference grid which possesses a small mesh size near the discontinuity and increases in size away from the discontinuity (both vertically and horizontally). This is accomplished if we transform the coordinates x and z by defining:

$$\hat{x} \equiv a_1 \ln \frac{x + a_2}{a_2} \tag{3.1}$$

and

$$\hat{z} \equiv b_1 \ln \frac{z + b_2}{b_2} + b_3 z \tag{3.2}$$

where $\hat{x}$ and $\hat{z}$ will assume only integer and half-integer values, and the quantities a_1, a_2, b_1, b_2, and b_3 are adjustable constants. The log-linear transformation on the vertical coordinate is, in part, motivated by the expected form of the wind profile under conditions of neutral atmospheric stability.

For the first derivative with respect to x we have:

$$\frac{\partial}{\partial x} = a_3 \frac{\partial}{\partial \hat{x}} \qquad \text{where} \qquad a_3 \equiv \frac{a_1}{a_2\, e^{\hat{x}/a_1}} \tag{3.3}$$

The first and second derivatives with respect to z become:

$$(3.4)\quad \frac{\partial}{\partial z} = \ell_4 \frac{\partial}{\partial \hat{z}} \qquad \text{where} \qquad \ell_4 \equiv \frac{b_1}{z + b_2} + b_3$$

and

$$(3.5)\quad \frac{\partial^2}{\partial z^2} = \ell_4^2 \frac{\partial^2}{\partial \hat{z}^2} - \ell_5 \frac{\partial}{\partial \hat{z}} \qquad \text{where} \qquad \ell_5 \equiv \frac{b_1}{(z + b_2)^2}$$

It should be noted that a_3 is a function of the horizontal coordinate, while ℓ_4 and ℓ_5 depend on the vertical coordinate.

With the coordinate transformation equations (3.3) through (3.5), the equations (2.16) through (2.19) become:

$$(3.6)\quad \frac{\partial u}{\partial t} = -\left(u\, a_3 \frac{\partial u}{\partial \hat{x}} + w\, \ell_4 \frac{\partial u}{\partial \hat{z}}\right) + f\,(v - v_g)$$

$$+ a_3 \frac{\partial}{\partial \hat{x}}\left(K_x\, a_3 \frac{\partial u}{\partial \hat{x}}\right) + \ell_4 \frac{\partial}{\partial \hat{z}}\left(K_z\, \ell_4 \frac{\partial u}{\partial \hat{z}}\right)$$

$$(3.7)\quad \frac{\partial v}{\partial t} = -\left(u\, a_3 \frac{\partial v}{\partial \hat{x}} + w\, \ell_4 \frac{\partial v}{\partial \hat{z}}\right) + f\,(u_g - u)$$

$$+ a_3 \frac{\partial}{\partial \hat{x}}\left(K_x\, a_3 \frac{\partial v}{\partial \hat{x}}\right) + \ell_4 \frac{\partial}{\partial \hat{z}}\left(K_z\, \ell_4 \frac{\partial v}{\partial \hat{z}}\right)$$

$$(3.8)\qquad \frac{\partial^2 w}{\partial \hat{z}^2} - \left(\frac{b_5}{b_4^2} + \frac{g\rho}{p b_4}\right)\frac{\partial w}{\partial \hat{z}} = \frac{\kappa \rho g a_3}{p b_4^2}\cdot\frac{\partial u}{\partial \hat{x}}$$

$$- \frac{a_3}{b_4}\frac{\partial}{\partial \hat{x}}\left(\frac{\partial u}{\partial \hat{z}}\right) + \frac{\rho(1-\kappa)f}{p b_4}\left(u_g \frac{\partial v}{\partial \hat{z}} - v_g \frac{\partial u}{\partial \hat{z}}\right)$$

$$(3.9)\qquad K_z = \ell^2 b_4 \left[\left(\frac{\partial u}{\partial \hat{z}}\right)^2 + \left(\frac{\partial v}{\partial \hat{z}}\right)^2\right]^{1/2}$$

with ℓ given by (2.20) and (2.21).

We may write equations (3.6) and (3.7) symbolically as

$$(3.10)\qquad \frac{\partial u}{\partial t} = GU + HU + FU$$

$$(3.11)\qquad \frac{\partial v}{\partial t} = GV + HV + FV$$

where the terms on the right of (3.10) and (3.11) represent the advective terms (GU and GV), the coriolis terms (HU and HV) and the frictional terms (FU and FV).

Thus,

$$(3.12)\qquad \begin{aligned} GU &\equiv - a_3 u \frac{\partial u}{\partial \hat{x}} - b_4 w \frac{\partial u}{\partial \hat{z}} \\ GV &\equiv - a_3 u \frac{\partial v}{\partial \hat{x}} - b_4 w \frac{\partial v}{\partial \hat{z}} \end{aligned}$$

$$
(3.13) \qquad \begin{aligned} HU &\equiv f\,(v - v_g) \\ HV &\equiv f\,(u_g - u) \end{aligned}
$$

$$
(3.14) \qquad \begin{aligned} FU &\equiv a_3 \frac{\partial}{\partial \hat{x}}\left(K_x\, a_3 \frac{\partial u}{\partial \hat{x}}\right) + b_4 \frac{\partial}{\partial \hat{z}}\left(K_z\, b_4 \frac{\partial u}{\partial \hat{z}}\right) \\ FV &\equiv a_3 \frac{\partial}{\partial \hat{x}}\left(K_x\, a_3 \frac{\partial v}{\partial \hat{x}}\right) + b_4 \frac{\partial}{\partial \hat{z}}\left(K_z\, b_4 \frac{\partial v}{\partial \hat{z}}\right) \end{aligned}
$$

For the advective terms, (3.12), we shall use upstream differencing; that is, for point jk (see grid below), if $u > o$ (i.e., in the direction of increasing $\hat{x}$) we have:

$$
a_3 u \frac{\partial u}{\partial \hat{x}} \doteq (a_3 u)_{jk} \frac{u_{jk} - u_{j-1\,k}}{\Delta \hat{x}}
$$

$$
\doteq (a_3 u)_{jk} (u_{jk} - u_{j-1\,k})
$$

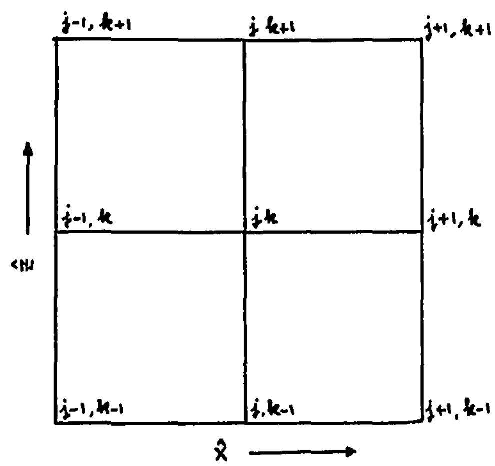

since $\Delta \hat{x} = 1$ over one grid distance. For $u < o$ we would have

$$
a_3 u \frac{\partial u}{\partial \hat{x}} \doteq (a_3 u)_{jk} (u_{j+1\,k} - u_{jk})
$$

Complete expressions for GU and GV giving all of the advection possibilities are:

$$(3.15)\quad GU_{jk} = \begin{cases} -(a_3 u)_{jk}(u_{jk} - u_{j-1\,k}) - (b_4 w)_{jk}(u_{jk} - u_{jk-1}) & \text{for } u > 0,\ w > 0 \\ -(a_3 u)_{jk}(u_{jk} - u_{j-1\,k}) - (b_4 w)_{jk}(u_{jk+1} - u_{jk}) & \text{for } u > 0,\ w < 0 \\ -(a_3 u)_{jk}(u_{j+1\,k} - u_{jk}) - (b_4 w)_{jk}(u_{jk} - u_{jk-1}) & \text{for } u < 0,\ w > 0 \\ -(a_3 u)_{jk}(u_{j+1\,k} - u_{jk}) - (b_4 w)_{jk}(u_{jk+1} - u_{jk}) & \text{for } u < 0,\ w < 0 \end{cases}$$

$$(3.16)\quad GV_{jk} = \begin{cases} -(a_3 u)_{jk}(v_{jk} - v_{j-1\,k}) - (b_4 w)_{jk}(v_{jk} - v_{jk-1}) & \text{for } u > 0,\ w > 0 \\ -(a_3 u)_{jk}(v_{jk} - v_{j-1\,k}) - (b_4 w)_{jk}(v_{jk+1} - v_{jk}) & \text{for } u > 0,\ w < 0 \\ -(a_3 u)_{jk}(v_{j+1\,k} - v_{jk}) - (b_4 w)_{jk}(v_{jk} - v_{jk-1}) & \text{for } u < 0,\ w > 0 \\ -(a_3 u)_{jk}(v_{j+1\,k} - v_{jk}) - (b_4 w)_{jk}(v_{jk+1} - v_{jk}) & \text{for } u < 0,\ w < 0 \end{cases}$$

For the coriolis terms, (3.13), we have simply:

$$(3.17)\qquad HU_{jk} = f\,(v_{jk} - v_g)$$

$$(3.18)\qquad HV_{jk} = f\,(u_g - u_{jk})$$

For the friction terms we shall use ordinary centered differencing, such that:

$$\left(\frac{\partial u}{\partial \hat{x}}\right)_{j+\frac{1}{2}\,k} \doteq \frac{u_{j+1\,k} - u_{jk}}{\Delta \hat{x}} = (u_{j+1\,k} - u_{jk})$$

and

$$\left(\frac{\partial u}{\partial \hat{z}}\right)_{j\,k-\frac{1}{2}} \doteq \frac{u_{jk} - u_{j\,k-1}}{\Delta \hat{z}} = (u_{jk} - u_{j\,k-1})$$

The friction terms, (3.14), then become:

(3.19) $$FU_{jk} = (a_3)_{jk}\left[(K_x a_3)_{j+\frac{1}{2}\,k}(u_{j+1\,k} - u_{jk}) - (K_x a_3)_{j-\frac{1}{2}\,k}(u_{jk} - u_{j-1\,k})\right] + (b_4)_{jk}\left[(K_z b_4)_{j\,k+\frac{1}{2}}(u_{j\,k+1} - u_{jk}) - (K_z b_4)_{j\,k-\frac{1}{2}}(u_{jk} - u_{j\,k-1})\right]$$

(3.20) $$FV_{jk} = (a_3)_{jk}\left[(K_x a_3)_{j+\frac{1}{2}\,k}(u_{j+1\,k} - u_{jk}) - (K_x a_3)_{j-\frac{1}{2}\,k}(u_{jk} - u_{j-1\,k})\right] + (b_4)_{jk}\left[(K_z b_4)_{j\,k+\frac{1}{2}}(u_{j\,k+1} - u_{jk}) - (K_z b_4)_{j\,k-\frac{1}{2}}(u_{jk} - u_{j\,k-1})\right]$$

Forward time differencing will be used so that the velocities at time step n + 1 will be given in terms of time step n by:

(3.21) $$u^{m+1}_{jk} = u^{m}_{jk} + \left(GU^{m}_{jk} + HU^{m}_{jk} + FU^{m}_{jk}\right)\Delta t$$

(3.22) $$v^{m+1}_{jk} = v^{m}_{jk} + \left(GV^{m}_{jk} + HV^{m}_{jk} + FV^{m}_{jk}\right)\Delta t$$

For the special case of horizontal homogeneity, the advective terms are zero, and the frictional expressions contain only those terms involving K_z .

The finite difference analog to equation (3.8) is obtained by replacing the differential operations with centered differences. This yields, after rearrangement and collection of terms:

$$(3.23)\quad \left[\frac{1}{4}\left(\frac{b_5}{b_4^2}+\frac{g\rho}{p b_4}-2\right)w\right]_{jk+1}+w_{jk}-\left[\frac{1}{4}\left(\frac{b_5}{b_4^2}+\frac{g\rho}{p b_4}+2\right)w\right]_{jk-1}$$

$$=\frac{1}{8}\left(\frac{a_3}{b_4}\right)_{jk}\left(u_{j+1\,k+1}+u_{j-1\,k-1}-u_{j-1\,k+1}-u_{j+1\,k-1}\right)-\frac{\kappa\rho g}{4p}\left(\frac{a_3}{b_4^2}\right)_{jk}\left(u_{j+1\,k}-u_{j-1\,k}\right)$$

$$-\frac{\rho(1-\kappa)f}{4p\,(b_4)_{jk}}\left[u_g\left(v_{jk+1}-v_{jk-1}\right)-v_g\left(u_{jk+1}-u_{jk-1}\right)\right]$$

which is in an implicit form suitable for solution by line iterative techniques (Richtmeyer (1957), p. 101; Forsythe and Wasow (1960), p. 104). For an incompressible atmosphere, all terms involving the density in (3.23) would cancel.

The finite difference representation of (3.9), using centered differences, is:

$$(3.24)\quad \left(K_z\right)_{jk+\frac{1}{2}}=\left(\ell^2 b_4\right)_{jk+\frac{1}{2}}\left[\left(u_{jk+1}-u_{jk}\right)^2+\left(v_{jk+1}-v_{jk}\right)^2\right]^{1/2}$$

Equations (3.21), (3.22), (3.23), and (3.24) form the basic set which is to be solved. A unique solution cannot be obtained, however, until boundary conditions on the variables u , v , and w are specified. We shall assume no-slip conditions to prevail at the horizontal, impenetrable earth's surface, hence $u = v = w = 0$ at $z = 0$. For the upper boundary condition we require the wind to become geostrophic at the highest grid point (selected near a height of one kilometer). This gives $u = u_g$, $v = v_g$, and $w = 0$ at the upper boundary. It is also frequently convenient to orient the x-axis such that $v_g = 0$. For the lateral boundaries we require the horizontal gradients of the horizontal velocity components and also the vertical velocity to vanish.

The boundary conditions may be summarized as follows:

Upper boundary conditions:

$$u = u_g \quad , \quad v = v_g \quad , \quad w = 0$$

Lateral boundary conditions:

$$\frac{\partial u}{\partial x} = \frac{\partial v}{\partial x} = 0 \quad , \quad w = 0$$

Lower boundary conditions:

$$u = v = w = 0$$

If we also assume an adiabatic temperature stratification and specify a value for pressure which is constant along the upper boundary, then the thermodynamic variables which appear in equation (3.23) may be calculated.

IV. STABILITY ANALYSIS

Whatever the particular atmospheric model chosen, the determination of its future state is an initial-value problem. The state of the atmosphere is specified at some initial time, t_o . A solution exists for $t \geqslant t_o$, and is uniquely determined by the governing equations together with the boundary conditions. However, when the partial differential equations are replaced by finite-difference quotients, a certain error is incurred. If, when the march in time is carried out for a fixed mesh size, a component of the error is amplified without bound, then the difference operator is said to be unstable. Instability in this sense is independent of round-off error, and is a property of the difference system as shown by Courant, Friedrichs and Lewy (1928). The following stability development will make liberal use of Richtmyer (1957).

Consider the linearized equations:

$$(4.1) \qquad \frac{\partial u}{\partial t} + \bar{u}\frac{\partial u}{\partial x} - f v = \frac{\partial K}{\partial z}\cdot\frac{\partial u}{\partial z} + K\frac{\partial^2 u}{\partial z^2}$$

$$(4.2) \qquad \frac{\partial v}{\partial t} + \bar{u}\frac{\partial v}{\partial x} + f u = \frac{\partial K}{\partial z}\cdot\frac{\partial v}{\partial z} + K\frac{\partial^2 v}{\partial z^2}$$

These equations are similar in form to our basic equations for horizontal motion (2.17) and (2.18), but are sufficiently simplified so that a reasonably complete stability analysis can be made. If we take K to be a linear function of height ($K = B\,(z + z_o)$) with $B > 0$, then (4.1) and (4.2) become:

$$(4.3) \qquad \frac{\partial u}{\partial t} = f v - \bar{u}\frac{\partial u}{\partial x} + B\frac{\partial u}{\partial z} + K\frac{\partial^2 u}{\partial z^2}$$

$$(4.4) \qquad \frac{\partial v}{\partial t} = -fu - \bar{u}\frac{\partial v}{\partial x} + B\frac{\partial v}{\partial z} + K\frac{\partial^2 v}{\partial z^2}$$

Using a forward time difference, upstream differencing on the advection term and centered space differencing on the mixing terms gives, after slight rearrangement:

$$(4.5) \qquad u_{jk}^{m+1} = u_{jk}^{m} + f\Delta t\, v_{jk}^{m} - \frac{\bar{u}\Delta t}{\Delta x}\left(u_{jk}^{m} - u_{j-1\,k}^{m}\right)$$

$$+ \frac{B\Delta t}{2\Delta z}\left(u_{jk+1}^{m} - u_{jk-1}^{m}\right) + \frac{K\Delta t}{(\Delta z)^2}\left(u_{jk+1}^{m} + u_{jk-1}^{m} - 2u_{jk}^{m}\right)$$

$$(4.6) \qquad v_{jk}^{m+1} = v_{jk}^{m} - f\Delta t\, u_{jk}^{m} - \frac{\bar{u}\Delta t}{\Delta x}\left(v_{jk}^{m} - v_{j-1\,k}^{m}\right)$$

$$+ \frac{B\Delta t}{2\Delta z}\left(v_{jk+1}^{m} - v_{jk-1}^{m}\right) + \frac{K\Delta t}{(\Delta z)^2}\left(v_{jk+1}^{m} + v_{jk-1}^{m} - 2v_{jk}^{m}\right)$$

Assuming we may represent the spacial distribution of the velocities by trignonometric series and considering only a single harmonic of this Fourier series representation we may write:

$$u(x,z) = A(z)\, e^{imx}$$

hence

$$u(x-\Delta x, z) = A(z)\, e^{imx}\, e^{-im\Delta x}$$

which yields

$$u(x-\Delta x, z) = u(x, z)\, e^{-im\Delta x}$$

or

$$u_{j-1\,k} = u_{jk}\, e^{-im\Delta x}$$

Likewise

$$u_{jk-1} = u_{jk}\, e^{-in\Delta z}$$

and

$$u_{jk+1} = u_{jk}\, e^{in\Delta z}$$

Substitution into (4.5) and (4.6) yields:

$$(4.7) \quad u_{jk}^{n+1} = u_{jk}^{n}\Big[1 - \frac{\bar{u}\Delta t}{\Delta x}\left(1 - e^{-im\Delta x}\right) + \frac{B\Delta t}{2\Delta z}\left(e^{in\Delta z} - e^{-in\Delta z}\right)$$

$$+ \frac{K\Delta t}{(\Delta z)^2}\left(e^{in\Delta z} + e^{-in\Delta z} - 2\right)\Big] + f\Delta t\, v_{jk}^{n}$$

$$(4.8) \quad v_{jk}^{n+1} = v_{jk}^{n}\Big[1 - \frac{\bar{u}\Delta t}{\Delta x}\left(1 - e^{-im\Delta x}\right) + \frac{B\Delta t}{2\Delta z}\left(e^{in\Delta z} - e^{-in\Delta z}\right)$$

$$+ \frac{K\Delta t}{(\Delta z)^2}\left(e^{in\Delta z} + e^{-in\Delta z} - 2\right)\Big] - f\Delta t\, u_{jk}^{n}$$

Recalling Euler's formula for exponentials:

$$e^{-im\Delta x} = \cos(m\Delta x) - i\sin(m\Delta x)$$

we may write

$$(4.9) \qquad (1 - e^{-im\Delta x}) = 2 \sin^2 \frac{m\Delta x}{2} + i \sin m\Delta x$$

Also

$$(4.10) \qquad \frac{1}{2}\left(e^{in\Delta z} - e^{-in\Delta z}\right) = i \sin n\Delta z$$

and

$$(4.11) \qquad \frac{1}{2}\left(e^{in\Delta z} + e^{-in\Delta z}\right) = \cos n\Delta z$$

After substitution of (4.9) through (4.11), equations (4.7) and (4.8) become:

$$(4.12) \quad u_{jk}^{n+1} = u_{jk}^{n}\left[1 - \frac{\bar{u}\Delta t}{\Delta x}\left(2 \sin^2 \frac{m\Delta x}{2} + i \sin m\Delta x\right) + \frac{B\Delta t}{\Delta z} i \sin n\Delta z + \frac{2K\Delta t}{(\Delta z)^2}\left(\cos n\Delta z - 1\right)\right] + v_{jk}^{n} f \Delta t$$

$$(4.13) \quad v_{jk}^{n+1} = v_{jk}^{n}\left[1 - \frac{\bar{u}\Delta t}{\Delta x}\left(2 \sin^2 \frac{m\Delta x}{2} + i \sin m\Delta x\right) + \frac{B\Delta t}{\Delta z} i \sin n\Delta z + \frac{2K\Delta t}{(\Delta z)^2}\left(\cos n\Delta z - 1\right)\right] - u_{jk}^{n} f \Delta t$$

We may write $\cos n\Delta z - 1 = -2 \sin^2 \frac{n\Delta z}{2}$. In addition, it is convenient to define the quantities

$$(4.14) \qquad \beta \equiv \frac{\bar{u}\Delta t}{\Delta x} \quad ; \quad \alpha \equiv \frac{K\Delta t}{(\Delta z)^2} \quad ; \quad \gamma \equiv \frac{B\Delta t}{\Delta z}$$

$$\theta \equiv \frac{m\Delta x}{2} \quad ; \quad \phi \equiv \frac{n\Delta z}{2} \quad ; \quad \eta \equiv f\Delta t$$

where all of the defined quantities are greater than or equal to zero. Using (4.14), equations (4.12) and (4.13) may be written, after collecting real and imaginary parts:

$$(4.15) \quad u_{jk}^{n+1} = u_{jk}^{n}\left[\left(1-2\beta\sin^2\theta - 4\alpha\sin^2\phi\right) + i\left(\gamma\sin 2\phi - \beta\sin 2\theta\right)\right] - v_{jk}^{n}\eta$$

$$(4.16) \quad v_{jk}^{n+1} = v_{jk}^{n}\left[\left(1-2\beta\sin^2\theta - 4\alpha\sin^2\phi\right) + i\left(\gamma\sin 2\phi - \beta\sin 2\theta\right)\right] + u_{jk}^{n}\eta$$

Now we define

$$(4.17) \qquad \sigma \equiv \left(1 - 2\beta\sin^2\theta - 4\alpha\sin^2\phi\right)$$

$$(4.18) \qquad \mu \equiv \left(\gamma\sin 2\phi - \beta\sin 2\theta\right)$$

which gives

$$(4.19) \qquad u_{jk}^{n+1} = u_{jk}^{n}\left(\sigma + i\mu\right) - v_{jk}^{n}\eta$$

$$(4.20) \qquad v_{jk}^{n+1} = v_{jk}^{n}\left(\sigma + i\mu\right) + u_{jk}^{n}\eta$$

Dropping the subscripts and writing (4.19) and (4.20) in matrix form yields:

$$(4.21)\qquad \begin{pmatrix} u^{n+1} \\ v^{n+1} \end{pmatrix} = \begin{pmatrix} \sigma + i\mu & -\eta \\ \eta & \sigma + i\mu \end{pmatrix} \cdot \begin{pmatrix} u^{n} \\ v^{n} \end{pmatrix}$$

The amplification matrix G is thus:

$$(4.22)\qquad G = \begin{pmatrix} \sigma + i\mu & -\eta \\ \eta & \sigma + i\mu \end{pmatrix}$$

In order to explicitly state our stability criteria, we need to know if G is a normal matrix. We determine this by evaluating the products GG^* and G^*G where

$$G^* = \begin{pmatrix} \sigma - i\mu & \eta \\ -\eta & \sigma - i\mu \end{pmatrix}$$

is the tranpose of the conjugate of G. We find that $GG^* = G^*G$ which is necessary and sufficient to insure that the matrix G is normal.

For a normal amplification matrix, the von Neumann necessary condition for stability is also sufficient (Richtmyer (1957), p. 61). This condition may be written:

$$(4.23)\qquad |\lambda^{(i)}| \leq 1 + O(\Delta t)$$

where $|\lambda^{(i)}|$ represents the absolute value of each of the i eigenvalues of the amplification matrix G . The term $O(\Delta t)$

is read "terms of first order in Δt " and permits "legitimate" exponential growth (Richtmyer, p. 60-61).

The eigenvalues of the matrix G may be found from the roots of the characteristic equation:

$$(4.24) \qquad \det(G - \lambda I) = \begin{vmatrix} \sigma + i\mu - \lambda & -\eta \\ \eta & \sigma + i\mu - \lambda \end{vmatrix} = 0$$

or

$$(\sigma + i\mu - \lambda)^2 + \eta^2 = 0$$

Hence:

$$\lambda^{(1)} = \sigma + i(\mu - \eta)$$

$$\lambda^{(2)} = \sigma + i(\mu + \eta)$$

and

$$(4.25) \qquad \mathrm{Max}\,|\lambda| = \left[\sigma^2 + (\mu + \eta)^2\right]^{1/2}$$

The von Neumann necessary and sufficient condition for stability may then be written:

$$(4.26) \qquad \left[\sigma^2 + (\mu + \eta)^2\right]^{1/2} \leq 1 + O(\Delta t)$$

for σ , μ , and $\eta > 0$.

Expanding the left side of (4.26) by using the definitions (4.17) and (4.18) yields:

$$(4.27) \qquad \left[(1 - 2\beta\sin^2\theta - 4\alpha\sin^2\phi)^2 + (\gamma\sin 2\phi - \beta\sin 2\theta + \eta)^2\right]^{1/2}$$

$$\leq 1 + O(\Delta t)$$

We shall now investigate the requirements for stability as set forth by equation (4.27) for a number of special cases.

Case 1

We take $\beta = \gamma = 0$, $\alpha \neq 0$ which implies $\bar{u} = 0$ and K = constant (i.e. $B = 0$). Equation (4.27) reduces to

$$(4.28) \quad \left[(1 - 4\alpha \sin^2 \phi)^2 + \eta^2 \right]^{1/2} \leq 1 + O(\Delta t)$$

Since

$$(4.29) \quad \left[(1 - 4\alpha \sin^2 \phi)^2 + \eta^2 \right]^{1/2} \leq |(1 - 4\alpha \sin^2 \phi)| + |\eta|$$

we could use as our stability criteria the equally valid, but more restrictive expression:

$$(4.30) \qquad |1 - 4\alpha \sin^2 \phi| + |\eta| \leq 1 + O(\Delta t)$$

Although it is conceivable that this might be too restrictive to be of value, we fir… that, in general,

$$|\eta| << |\sigma| \text{ or } |\mu|$$

and expression (4.29) is very nearly an equality.

We may then combine $\eta \equiv f \Delta t$ with the $O(\Delta t)$ term on the right side of (4.30) with the result

$$|1 - 4\alpha \sin^2 \phi| \leq 1 + O(\Delta t)$$

which is satisfied for all ϕ if $2\alpha \leq 1$ or, substituting for α from (4.14),

$$(4.31) \qquad \frac{2K\Delta t}{(\Delta z)^2} \leq 1$$

This is the expected result for the solution of the linear diffusion equation in one dimension with constant coefficients (Richtmyer (1957), p. 13).

Case 2

When $\beta = 0$, $\alpha \neq 0$, $\gamma \neq 0$ expression (4.27) reduces to:

$$(4.32) \quad \left[(1 - 4\alpha \sin^2\phi)^2 + (\gamma \sin 2\phi + \eta)^2\right]^{1/2} \leq 1 + O(\Delta t)$$

We will assume α constant as Δt and Δx approach zero so that (4.32) may be written (substituting for γ and η):

$$\left[(1 - 4\alpha \sin^2\phi)^2 + \left(\frac{B\Delta t}{\Delta z} \sin 2\phi + f\,\Delta t\right)^2\right]^{1/2} \leq 1 + O(\Delta t)$$

or

$$(4.33) \quad \left[(1 - 4\alpha \sin^2\phi)^2 + \left(\frac{B}{\Delta z} \sin 2\phi + f\right)^2 (\Delta t)^2\right]^{1/2} \leq 1 + O(\Delta t)$$

To satisfy (4.33) we must at least require

$$(1 - 4\alpha \sin^2\phi)^2 \leq 1$$

which for all ϕ results in the stability conditions as given by (4.31). If (4.31) is satisfied with the equality sign, and if M is the maximum with respect to ϕ of $\left(\frac{B}{\Delta z} \sin 2\phi + f\right)^2$

then (4.33) becomes at worst:

$$\left[1 + M(\Delta t)^2 \right]^{1/2} \leq 1 + O(\Delta t)$$

Thus, (4.31) is seen to be not only a necessary condition for stability but also a sufficient condition for both cases 1 and 2. The importance of this result cannot be overestimated for it shows that for a given independent variable, stability is determined by the highest order terms in the finite difference approximation to the partial differential equation. According to Richtmyer (p. 98), the presence of lower order terms might necessitate replacing $\Delta t \leq \ldots$ with $\Delta t < \ldots$, but no other changes should be necessary. We can then consider a general case in which $\gamma = 0$, $\alpha \neq 0$, $\beta \neq 0$.

Case 3

When $\gamma = 0$, $\beta \neq 0$, and $\alpha \neq 0$ expression (4.27) reduces to:

$$(4.34) \quad \left[(1 - 2\beta \sin^2\theta - 4\alpha \sin^2\phi)^2 + (-\beta \sin 2\theta + \eta)^2 \right]^{1/2} \leq 1 + O(\Delta t)$$

Subcase 3a

To satisfy (4.34) we must at least require

$$| 1 - 2\beta \sin^2\theta - 4\alpha \sin^2\phi | \leq 1$$

This is satisfied for all θ and ϕ if $(\beta + 2\alpha) \leq 1$.
Substituting for α and β from (4.14) yields:

$$(4.35) \qquad \frac{\bar{u}\,\Delta t}{\Delta x} + \frac{2K\Delta t}{(\Delta z)^2} \leq 1$$

Subcase 3b

For a given value of β, the second term in the brackets of (4.34) has a maximum value when $\sin 2\theta = -1$, which gives $\sin^2\theta = 1/2$. For the case when $\sin^2\phi = 0$ we obtain:

$$[(1-\beta)^2 + (\beta+\eta)^2]^{1/2} \leq 1 + O(\Delta t)$$

We approximate this by assuming $\eta << \beta$ which gives

$$[(1 - 2\beta + 2\beta^2]^{1/2} \leq 1 + O(\Delta t)$$

This is satisfied if $\beta \leq 1$ or

$$(4.36) \qquad \frac{\bar{u}\,\Delta t}{\Delta x} \leq 1$$

For $\sin^2\phi = 1$ we have from (4.34)

$$[(1-\beta-4\alpha)^2 + (\beta+\eta)^2]^{1/2} \leq 1 + O(\Delta t)$$

We approximate this by

$$(4.37) \qquad [(1-(\beta+4\alpha))^2 + \beta^2]^{1/2} \leq 1 + O(\Delta t)$$

The left side of (4.37) can be written:

$$\left[(1-\beta-4\alpha)^2+\beta^2\right]^{1/2} \leq |1-\beta-4\alpha| + |\beta|$$

Stability should be insured, then, if $|1-\beta-4\alpha|+|\beta| \leq 1+O(\Delta t)$
If we "add" $|\beta|$ into $|1-\beta-4\alpha|$ we get $|1-4\alpha| \leq 1+O(\Delta t)$
which is satisfied by (4.31). If we "subtract" $|\beta|$ into $|1-\beta-4\alpha|$ we have $|1-2(\beta+2\alpha)| \leq 1+O(\Delta t)$, which is satisfied by (4.35). It would appear then, that (4.35) is necessary and sufficient to insure stability.

We conclude that for the simplified equation considered in this chapter the finite differencing scheme used will be computationally stable if

(4.38) $$\Delta t < \frac{1}{\left(\frac{\bar{u}}{\Delta x} + \frac{2K}{(\Delta z)^2}\right)}$$

throughout the region of integration. This is usually a good approximation for the more general non-linear equation with variable coefficients.

V. TRUNCATION ERROR AND CONSISTENCY

The truncation error is defined as the difference between the finite difference formulation and the differential equation. We shall investigate the truncation error associated with the differential equation (4.3) and the corresponding finite difference analogue equation (4.5). Consideration of the y component equation of motion and its finite difference analog leads to an identical result, thus only one component need be considered.

Assuming $u(x,z,t)$ to be a function with continuous partial derivatives, we may expand u in Taylor's series about j, k, and n giving:

$$u^{m}_{jk} = u_0$$

$$u^{m+1}_{jk} = u_0 + \Delta t\left(\frac{\partial u}{\partial t}\right)^{m}_{jk} + \frac{(\Delta t)^2}{2!}\left(\frac{\partial^2 u}{\partial t^2}\right)^{m}_{jk} + \;.\;.\;.$$

$$u^{m}_{j-1\,k} = u_0 - \Delta x\left(\frac{\partial u}{\partial x}\right)^{m}_{jk} + \frac{(\Delta x)^2}{2!}\left(\frac{\partial^2 u}{\partial x^2}\right)^{m}_{jk} - + \;.\;.\;.$$

$$u^{m}_{jk+1} = u_0 + \Delta z\left(\frac{\partial u}{\partial z}\right)^{m}_{jk} + \frac{(\Delta z)^2}{2!}\left(\frac{\partial^2 u}{\partial z^2}\right)^{m}_{jk} + \;.\;.\;.$$

The truncation error $\epsilon[u]$ is the difference between equations (4.5) and (4.3). Substituting the series expansions into (4.5) results in

$$\epsilon[u] = \Bigg[\left(\frac{\partial u}{\partial t} + \frac{\Delta t}{2!}\frac{\partial^2 u}{\partial t^2} + \ldots\right)_0 + \bar{u}\left(\frac{\partial u}{\partial x} - \frac{\Delta x}{2!}\frac{\partial^2 u}{\partial x^2} + - \ldots\right)_0$$

$$- B\left(\frac{\partial u}{\partial z} + \frac{(\Delta z)^2}{3!}\frac{\partial^3 u}{\partial z^3} + \ldots\right)_0 - K\left(\frac{\partial^2 u}{\partial z^2} + \frac{(\Delta z)^2}{12}\frac{\partial^4 u}{\partial z^4} + \ldots\right)_0$$

$$- f v_0\Bigg] - \left[\frac{\partial u}{\partial t} + \bar{u}\frac{\partial u}{\partial x} - f v - B\frac{\partial u}{\partial z} - K\frac{\partial^2 u}{\partial z^2}\right]_0$$

which reduces to

$$\epsilon[u] = \left(\frac{\Delta t}{2!}\frac{\partial^2 u}{\partial t^2} + \ldots\right) - \bar{u}\left(\frac{\Delta x}{2!}\frac{\partial^2 u}{\partial x^2} + \ldots\right)$$

$$- B\left(\frac{(\Delta z)^2}{3!}\frac{\partial^3 u}{\partial z^3} + \ldots\right) - K\left(\frac{(\Delta z)^2}{12}\frac{\partial^4 u}{\partial z^4} + \ldots\right)$$

Thus, the truncation error may be written as

$$(5.1) \qquad \epsilon[u] = O(\Delta t) + O(\Delta x) + O(\Delta z)^2$$

If the truncation error tends to zero uniformly as $\Delta x, \Delta z, \Delta t \rightarrow 0$ then the difference equation is said to be a consistent approximation to the differential equation. This is accomplished if $\Delta t \rightarrow 0$ as $\Delta x \rightarrow 0$ and $(\Delta z)^2 \rightarrow 0$, which implies a functional relation of the form $\Delta t = h(\Delta x, (\Delta z)^2)$. This is precisely the form found in the preceding section and given by equation (4.35) or (4.38) as

$$\Delta t\left(\frac{\bar{u}}{\Delta x} + \frac{2K}{(\Delta z)^2}\right) \leq 1$$

or

$$\Delta t \leq \frac{(\Delta x)(\Delta z)^2}{\bar{u}(\Delta z)^2 + 2K(\Delta x)}$$

Thus, we may conclude that the difference equation is a consistent approximation to the differential equation. If we assume that our initial value problem is properly posed, as defined by Richtmyer

(p. 39-40 and p. 52-53), then the Lax equivalence theorem states that "...for a properly posed initial-value problem and an approximation satisfying the consistency condition, stability is necessary and sufficient for convergence." (Richtmyer (1957), p. 78).

The derivations and associated statements in this and the preceding chapter are based on an examination of a set of linear equations with constant coefficients. It has not been possible to perform similar analyses with non-linear equations and variable coefficients. In practice, however, the stability and consistency criteria as obtained from the linearized equations are used as a first approximation to the non-linear problem. Further refinement of the stability criteria can be made by trial and error; however, as found in our case, the final results frequently differ very little from those obtained from the linearized equations.

VI. COMPARISON WITH KNOWN SOLUTIONS

Analytical solutions to the differential equations which describe the wind structure in the atmospheric boundary layer can be obtained only after a number of simplifying assumptions are made. The results, however, are of importance to the current problem in two ways: (a) within the limitations of the assumptions, they show the general form of the boundary layer wind distribution which one might expect, and (b) they provide a simple and effective way in which to evaluate the degree to which the exact solution of the differential equations are duplicated by their finite difference analogues.

It is necessary to assume horizontal homogeneity and steady state. We shall also assume the geostrophic wind components to be constant with height. The equations of motion for two-dimensional mean flow become:

$$f(v - v_g) + \frac{\partial}{\partial z}\left(K_z \frac{\partial u}{\partial z}\right) = 0 \tag{6.1}$$

$$f(u_g - u) + \frac{\partial}{\partial z}\left(K_z \frac{\partial v}{\partial z}\right) = 0 \tag{6.2}$$

The solution obtained from equations (6.1) and (6.2) is dependent upon the height distribution of the eddy viscosity K_z. The two cases which will be considered are: (a) constant K_z, and (b) K_z a linear function of height.

The case of constant eddy viscosity in the atmospheric boundary layer was first investigated by Taylor (1915). If the x-axis is oriented along the geostrophic wind, then (6.1) and (6.2) become

(6.3) $$f v + K_z \frac{d^2 u}{d z^2} = 0$$

(6.4) $$f(u_g - u) + K_z \frac{d^2 v}{d z^2} = 0$$

Multiplying (6.4) by $i = \sqrt{-1}$, adding the result to (6.3), and defining $V \equiv u + iv$ gives

(6.5) $$\frac{d^2 V}{d z^2} - \frac{i f}{K_z}(V - u_g) = 0$$

For the boundary conditions

$$V = 0 \quad \text{on} \quad z = 0$$

$$\text{and} \lim_{z \to \infty} V = u_g$$

The solution of (6.5) is

(6.6) $$u = u_g(1 - e^{-\varsigma} \cos \varsigma)$$

(6.7) $$v = u_g(e^{-\varsigma} \sin \varsigma)$$

where $\varsigma \equiv z\sqrt{\dfrac{f}{2K_z}}$

The angle at any height between the actual wind and the geostrophic wind is given by

$$(6.8) \qquad \alpha = \tan^{-1}\frac{v}{u} = \frac{\sin \varsigma}{e^{\varsigma} - \cos \varsigma}$$

Using L'Hopital's rule we find $\alpha \to \pi/4$ as $z \to 0$. The resulting wind distribution given by (6.6) and (6.7) resembles the equiangular spiral found by Ekman (1905) in his examination of similar problems in the ocean, and as a result, is frequently referred to as the Ekman spiral solution to the boundary layer wind distribution.

The case when K_z is a linear function of height has been treated by Ellison (1956). Following his development, we multiply (6.1) by $i = \sqrt{-1}$, add the result to (6.2) and define $W \equiv u_g - u + i\,(v - v_g)$ which gives:

$$(6.9) \qquad ifW + \frac{\partial}{\partial z}\left(K_z \frac{\partial W}{\partial z}\right) = 0$$

For $K_z = k\,u_*\,(z + z_0)$ where k is von Karman's constant and u_* the (constant) friction velocity, (6.9) becomes

$$(6.10) \qquad \frac{\partial^2 W}{\partial z^2} + \frac{1}{z+z_0}\frac{\partial W}{\partial z} + \frac{if}{k\,u_*(z+z_0)} W = 0$$

Now let $X \equiv \sqrt{\dfrac{4f\,(z+z_0)}{k\,u_*}}$. Employing the transformation equations

$$\frac{\partial W}{\partial z} = \frac{\partial W}{\partial X}\cdot\frac{\partial X}{\partial z} = \sqrt{\frac{f}{k\,u_*(z+z_0)}}\;\frac{\partial W}{\partial X}$$

and

$$\frac{d^2 W}{dz^2} = \frac{f}{k u_* (z+z_0)} \cdot \frac{d^2 W}{dX^2} - \sqrt{\frac{f}{4 k u_* (z+z_0)^3}} \cdot \frac{dW}{dX}$$

equation (6.10) reduces to

$$\text{(6.11)} \qquad \frac{d^2 W}{dX^2} + \frac{1}{X} \cdot \frac{dW}{dX} + iW = 0$$

This is of standard form (Jahnke and Emde (1945), p. 146) with solution

$$W = \mathfrak{Z}_0(X\sqrt{i})$$

where $\mathfrak{Z}_0(X\sqrt{i})$ represents a linear combination of two independent solutions to equation (6.11). If we write the solution in terms of Hankel functions of zero order and first and second kind we have, where A and B are constants

$$\text{(6.12)} \qquad W = A \cdot H_0^{(1)}(X\sqrt{i}) + B \cdot H_0^{(2)}(X\sqrt{i})$$

Since $X > 0$ we know

$$H_0^{(1)}(X\sqrt{i}) \longrightarrow 0 \qquad \text{as} \quad X \longrightarrow \infty$$

$$H_0^{(2)}(X\sqrt{i}) \longrightarrow \infty \qquad \text{as} \quad X \longrightarrow \infty$$

The upper boundary condition requires the wind to approach the geostrophic value as $z \longrightarrow \infty$, hence $B = 0$ and we have from (6.12)

(6.13) $$W = A H_0^{(1)}(X\sqrt{i})$$

Representing $H_0^{(1)}(X\sqrt{i})$ in terms of Bessel functions of zero order and first and second kind

$$H_0^{(1)}(X\sqrt{i}) = J_0(X\sqrt{i}) + i\,Y_0(X\sqrt{i})$$

For small arguments

$$J_0(X\sqrt{i}) \doteq 1$$

$$i\,Y_0(X\sqrt{i}) \doteq \frac{2}{\pi} i\left(\gamma + \ln \frac{X\sqrt{i}}{2}\right)$$

where $\gamma \doteq 0.57722$ is Euler's constant. The Hankel function for small argument thus becomes

$$H_0^{(1)}(X\sqrt{i}) \doteq 1 + \frac{2}{\pi} i\left(\gamma + \ln X - \ln 2 + \ln\sqrt{i}\right)$$

But

$$\frac{2i}{\pi}\ln\sqrt{i} = \frac{2i}{\pi}\ln(e^{i\pi/4}) = -\frac{1}{2}$$

hence

(6.14) $$H_0^{(1)}(X\sqrt{i}) \doteq \frac{1}{2} + \frac{2i}{\pi}\left(\ln X - \ln 2 + \gamma\right)$$

For small X, (6.13) becomes

(6.15) $$W \doteq \frac{1}{2}A + \frac{2iA}{\pi}\left(\ln X - \ln 2 + \gamma\right)$$

Near the surface $v \to 0$ (the x-axis is oriented in the direction of the surface wind) and, for neutral atmospheric stability

$$u = \frac{u_*}{k} \ln \frac{z + z_0}{z_0} = \frac{u_*}{k} \ln \frac{k u_* X^2}{4 f z_0}$$

which may be written

$$(6.16) \qquad u = \frac{2 u_*}{k} \ln X + \frac{u_*}{k} \ln \frac{k u_*}{4 f z_0}$$

Since u_g and v_g are not functions of X, and $v = 0$ near the earth's surface we find, by comparing coefficients of $\ln X$ in (6.15) and (6.16) that $A = i\pi u_*/k$, hence

$$(6.17) \qquad \frac{k}{u_*}(u_g - i v_g) = \frac{\pi i}{2} + 2(\ln 2 - \gamma) + \ln \frac{k u_*}{4 f z_0}$$

Solving (6.17) for the magnitude of the geostrophic wind gives:

$$(6.18) \qquad \frac{k}{u_*}(u_g^2 + v_g^2)^{1/2} = \left[4(\ln 2 - \gamma)^2 + \left(\ln \frac{k u_*}{4 f z_0}\right)^2 + 4(\ln 2 - \gamma)\ln \frac{k u_*}{4 f z_0} + \frac{\pi^2}{4}\right]^{1/2}$$

We may also write the general solution for W:

$$(6.19) \qquad W = (u_g - u) + i(v - v_g) = \frac{i\pi u_*}{k} H_0^{(1)}(X\sqrt{i})$$

In a typical application of these equations (and the one that will be considered here), values are given for the geostrophic wind and surface roughness parameter. One can then compute u_* from (6.18). This allows X to be calculated. It is then a straightforward matter of using tabulated values of $H_0^{(1)}(X\sqrt{i})$ (Jahnke and Emde, (1945), p. 252) to determine W . Real and imaginary parts are then separated to give the velocity components u and v .

Analytical solutions may also be obtained for the case $K_z = K_1 \cdot z^{\nu}$ where K_1 is constant and $0 < \nu < 1$ (Möller (1931), Köhler (1933), and Frost (1948)). As in the preceding derivation, the solution is in terms of Bessel functions, though in this case, they are modified Bessel functions of the second kind of order $(1-\nu)/(2-\nu)$. Köhler's work is briefly summarized by Sutton (1953), p. 243). Brunt (1920) has also obtained analytic solutions for the two cases $\nu = 2$ and $\nu = 4$.

On the next few pages, analytical solutions will be given for the constant K_z and $K_z = k\, u_* (z + z_0)$ cases. Historical significance is attached to the former, while the latter is more physically significant. It is generally agreed that under conditions of neutral atmosphere stability, $K_z = k\, u_* (z + z_0)$ is consistent with the observed logarithmic wind profile (Lumley and Panofsky (1964)).

The solution for constant eddy viscosity has been obtained from equations (6.6) and (6.7) assuming $f = 10^{-4}$ sec^{-1}, $K_z = 20000$ cm^2 sec^{-1}, $u_g = 1000$ cm/sec and $v_g = 0$. The analytical solution is shown for u and v component velocities in Figure 1. Also shown in Figure 1 are numerical solutions obtained from two different sets of grid spacing. Numerical solutions were obtained by solving equations (3.21) and (3.22) for horizontally homogeneous conditions and K_z = constant = 20000 cm^2 sec^{-1}. In one case, the first grid point

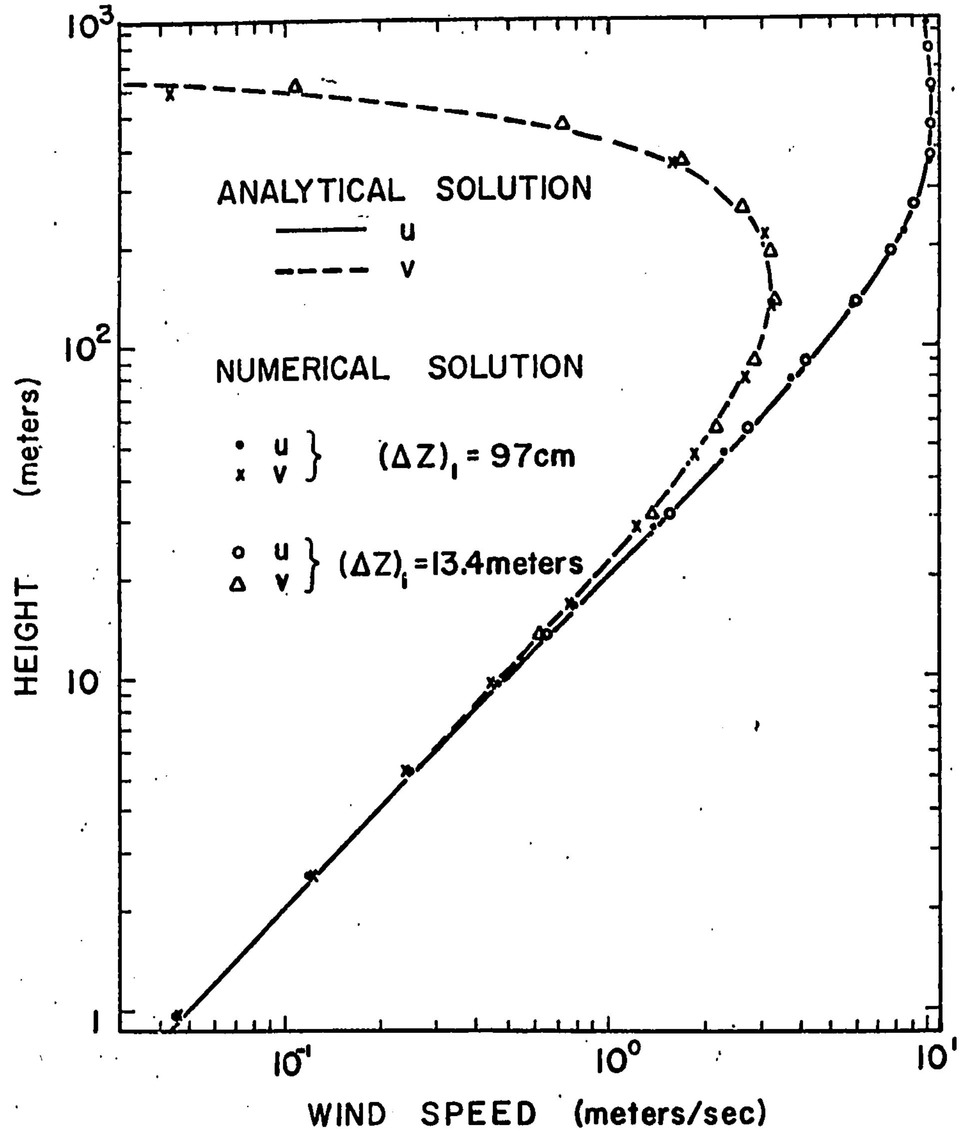

Fig. 1. Comparison of numerical and analytical solutions for K_z = 20000 cm^2/sec, U_g = 1000 cm/sec and two vertical grid spacings.

above the lower boundary is 97 cm and in the other, 13.4 meters. Computational stability by use of equation (4.38) is indicated for time steps of 0.2 and 15.0 seconds, respectively. For the type of problem under consideration, where the boundary conditions are constant, the solution obtained by numerical techniques will not be a function of the initial conditions. However, the number of time steps required to converge to the solution will be affected. In order to minimize the number of time steps, the analytical solutions were used as initial conditions for the numerical computations. Numerical integration of (3.21) and (3.22) was performed for two hours (36,000 time steps) for the smaller grid spacing and three hours (720 time steps) for the larger spacing. The resulting numerical solutions are seen to be in good agreement with the analytical solution both with regard to general shape of the profile and numerical values. Over most of the profile, the difference between numerical and analytical solutions is less than ten percent, and at many levels, less than five percent.

We now consider the case where the eddy viscosity is a linear function of height. Equation (6.18) yields a value of $u_* = 36.83$ cm/sec for $z_0 = 1$ cm, $f = 10^{-4}$ sec^{-1} and $(u_g^2 + v_g^2) = 1000$ cm/sec. Tables of Hankel functions (or (6.14) for small arguments) gives the analytical solution shown in Figure 2. This, and all other solutions to be presented have been adjusted so that the x-axis is oriented parallel to the geostrophic wind.

Figure 2 shows the effect of varying the vertical grid spacing. Because of the logarithmic structure of the wind, one would intuitively

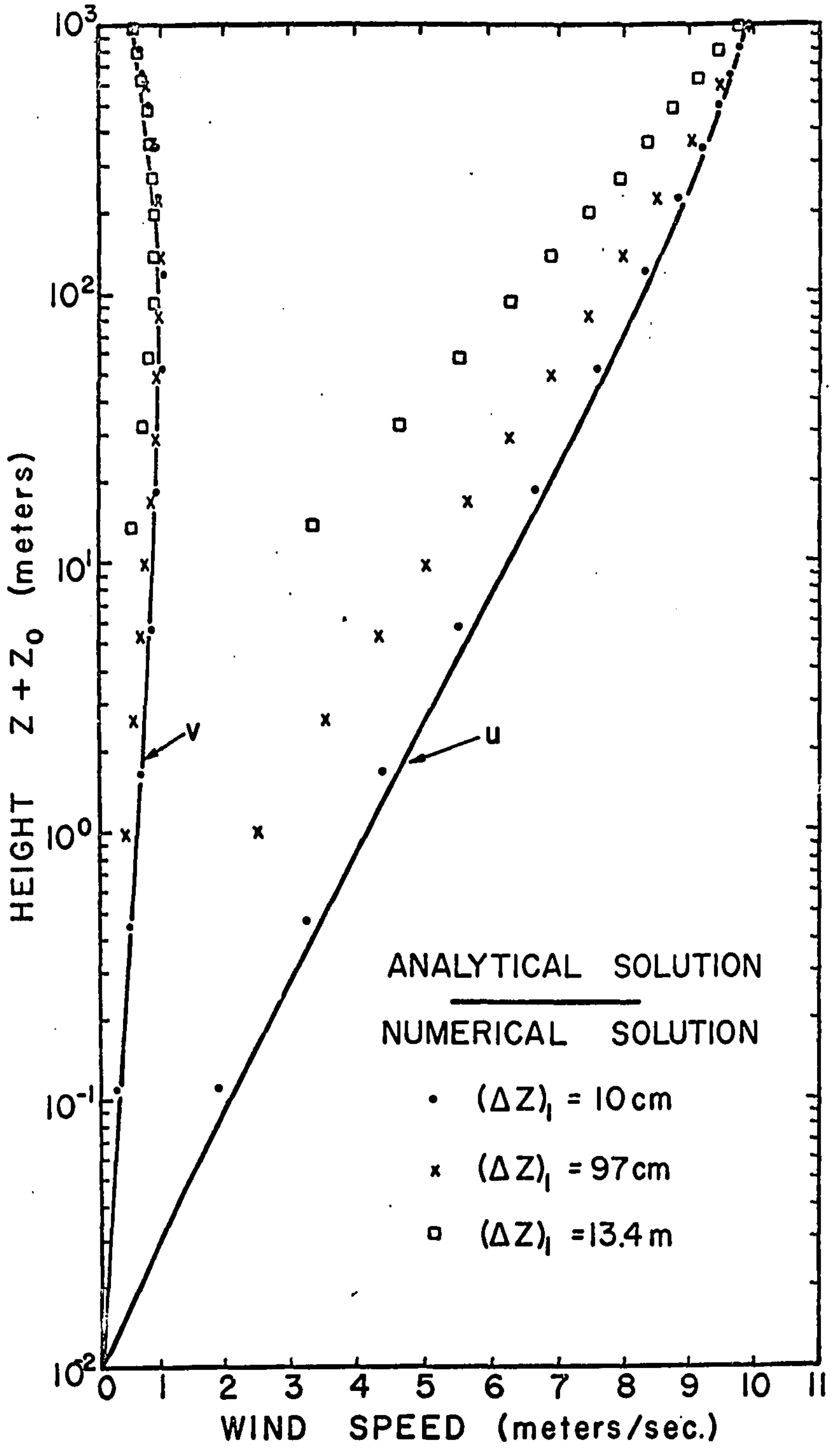

Fig. 2. Comparison of numerical and analytical solutions for $K_Z = k\ u_* \ (z + z_o)$, U_g = 1000 cm/sec, and three vertical grid spacings.

expect the distance between the lower grid points to be particularly important. This is borne out in the three cases shown, where we see the difference between the analytical and numerical solutions decreasing as we decrease the distance between the first two grid points from 13.4 meters to 97 cm and 10 cm. This general tendency could also have been predicted qualitatively from equation (5.1). The numerical results are obtained by using the analytical solution as initial input and integrating equations (3.21) and (3.22) for one hour. As a check to determine whether one hour was sufficient for the numerical scheme to converge to a steady solution, the case of $(\Delta z)_1 = 13.4$ meters was continued for two more hours. The computed values for u and v changed by less than 5 cm/sec during this two hour period, hence the one hour integration period was deemed sufficient. The truncation error due to the time-stepping interval was also investigated for this case. Time steps of 15 seconds and one second gave velocities after one hour which agreed within 0.4 cm/sec in u and 0.04 cm/sec in v.

In order to determine whether any significant bias in the integration results is introduced by using the analytical solution as initial input, one run was made which used initial conditions which differed significantly from the expected final solution, especially in the lower levels. Initial values for v were about one-fifth the analytical values up to $k = 7$ and initial values for u were approximately 100 cm/sec smaller than the analytic solution up to $k = 12$. The height corresponding to various k values are as given in Table 1, page 63. Although a longer integration time was required, the numerical solution converged to the same values as before; a result which is consistent with the Lax equivalence theorem mentioned in Chapter V and suggestive that the numerical scheme is consistent and properly posed.

It is unfortunate that there is such a large difference between the analytical and numerical solutions for the larger grid spacing. In order to obtain computational results which are in reasonable accord with theory, we are forced to choose a small grid spacing, and hence, from equation (4.38), a small time increment to maintain computational stability.

Figure 3 shows the analytical solution when $K_z = k\, u_* \,(z + z_0)$ for the four roughness parameter values of 1, 2, 5, and 10 cm. As before $u_g = 1000$ cm/sec, $v_g = 0$ and $f = 10^{-4}\ \mathrm{sec}^{-1}$. Also shown are the numerical results for the vertical grid spacing given in Table 1 (see page 63). The magnitude of the difference between the analytical and numerical solutions decreases with increasing roughness. This is to be expected since the rougher surface is associated with less curvature of the velocity profile in the lower layers, and hence is more accurately represented by the finite difference approximation. In all cases, the general shape of the profile is duplicated very well.

The percentage difference between the analytical and numerical solutions of Figure 3 is shown in Figure 4. As before, we use the analytical solution as initial conditions and integrate (3.21) and (3.22) for one hour. The largest percentage error of 12.1 percent

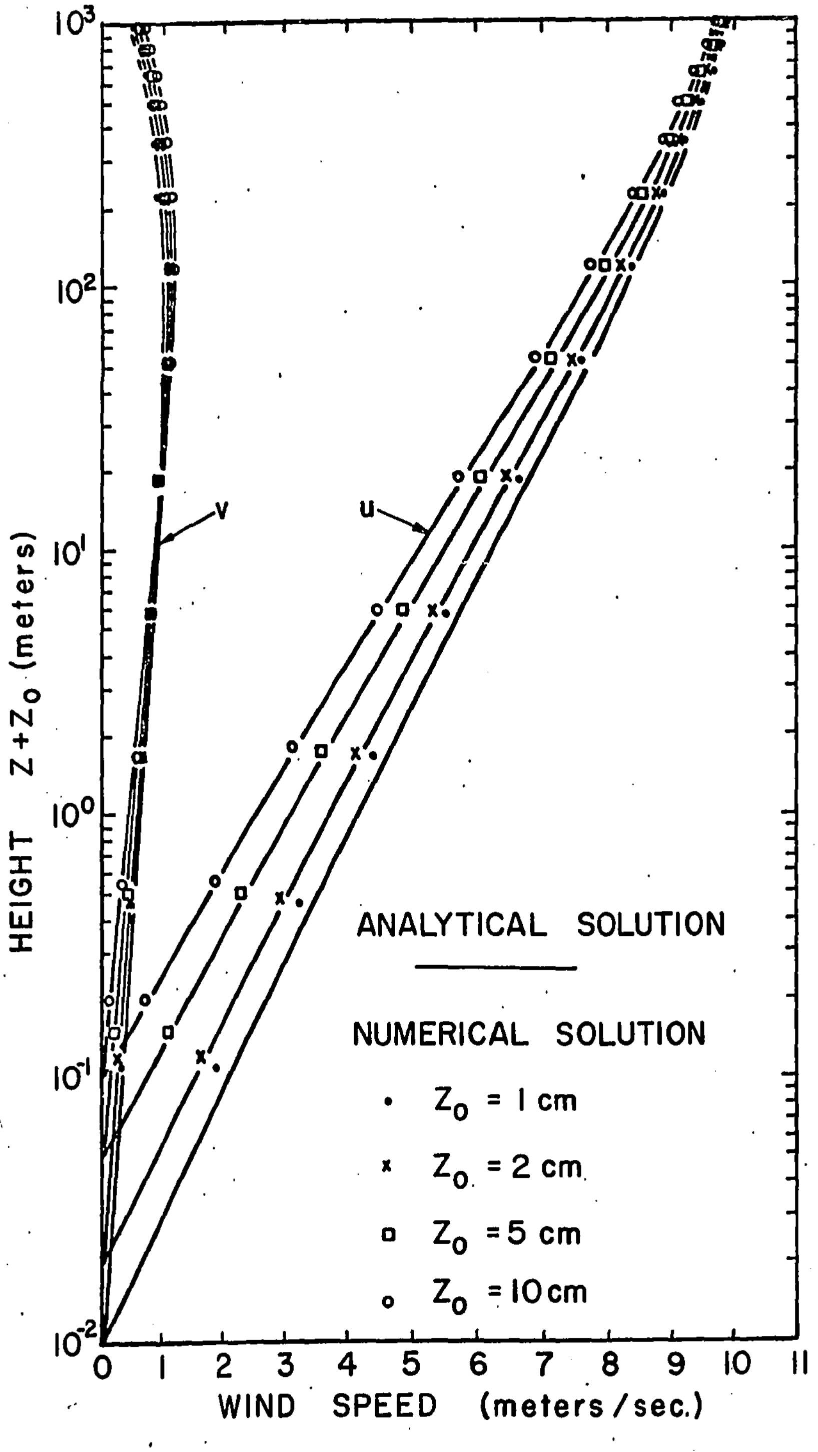

Fig. 3. Comparison of numerical and analytical solutions for $K_Z = k\, u_* \,(z + z_0)$, $U_g = 1000$ cm/sec, $(\Delta z)_1 = 10$ cm and roughness parameter values of 1, 2, 5, and 10 cm.

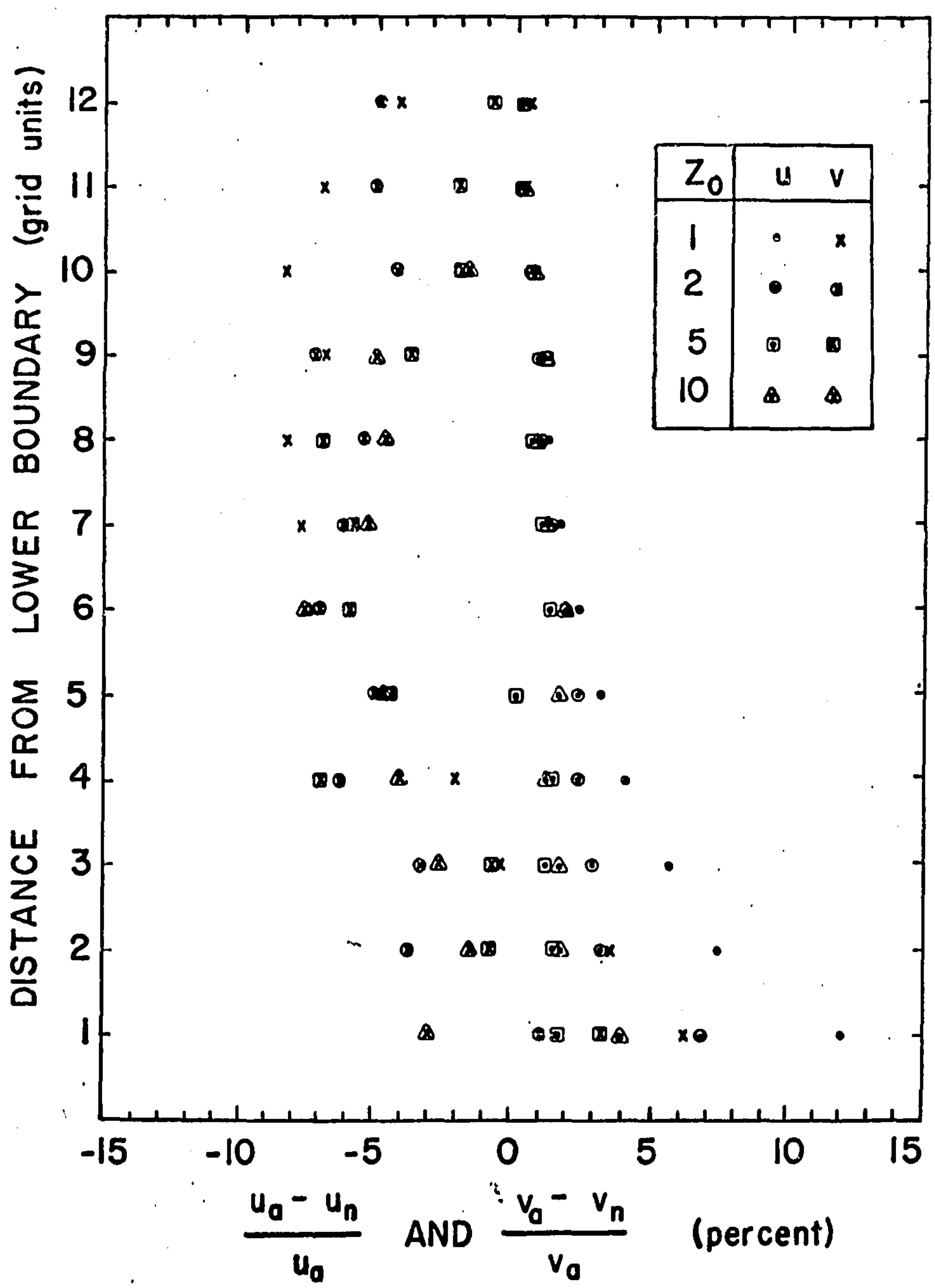

Fig. 4. Difference between analytical and numerical solutions for $K_z = k\, u_* \,(z + z_o)$ after starting with analytical solutions and integrating for one hour.

is associated with the lowest computed grid point for $z_0 = 1$ cm. All other values lie within $\pm$ 8 percent of the analytical solution.

An estimate of the degree to which steady state conditions have been achieved after the one hour integration period is indicated in Figure 5. Here we show the change in time of the x-component velocity over five minute periods. These curves are for a roughness parameter of 1 cm and selected elevations as indicated by the height index k, but they are typical of all other values. Convergence of the solution is apparent. From the curves presented in Figure 5 it appears that reasonably complete convergence to steady state conditions has been achieved after one hour.

We intend eventually to investigate the general character of the air flow when a change occurs in the surface roughness parameter. Thus, we should also look at how well the numerical scheme duplicates the analytical change in horizontal velocity for various changes in roughness. If we consider only the x-component of velocity as shown in Figure 3 and compute the difference in velocity at all heights for k equal to 2 through 13 as given in Table 1, we obtain the results shown in Figure 6. The velocity difference as computed from the analytical solution is plotted against that from the numerical solution. Perfect agreement would coincide with all data points lying on the line which appears in this figure. Reasonably good agreement is found between the analytical and numerical values.

One final comparison will be made. A computer program similar to that described by Blackadar (1962) has been written and solved

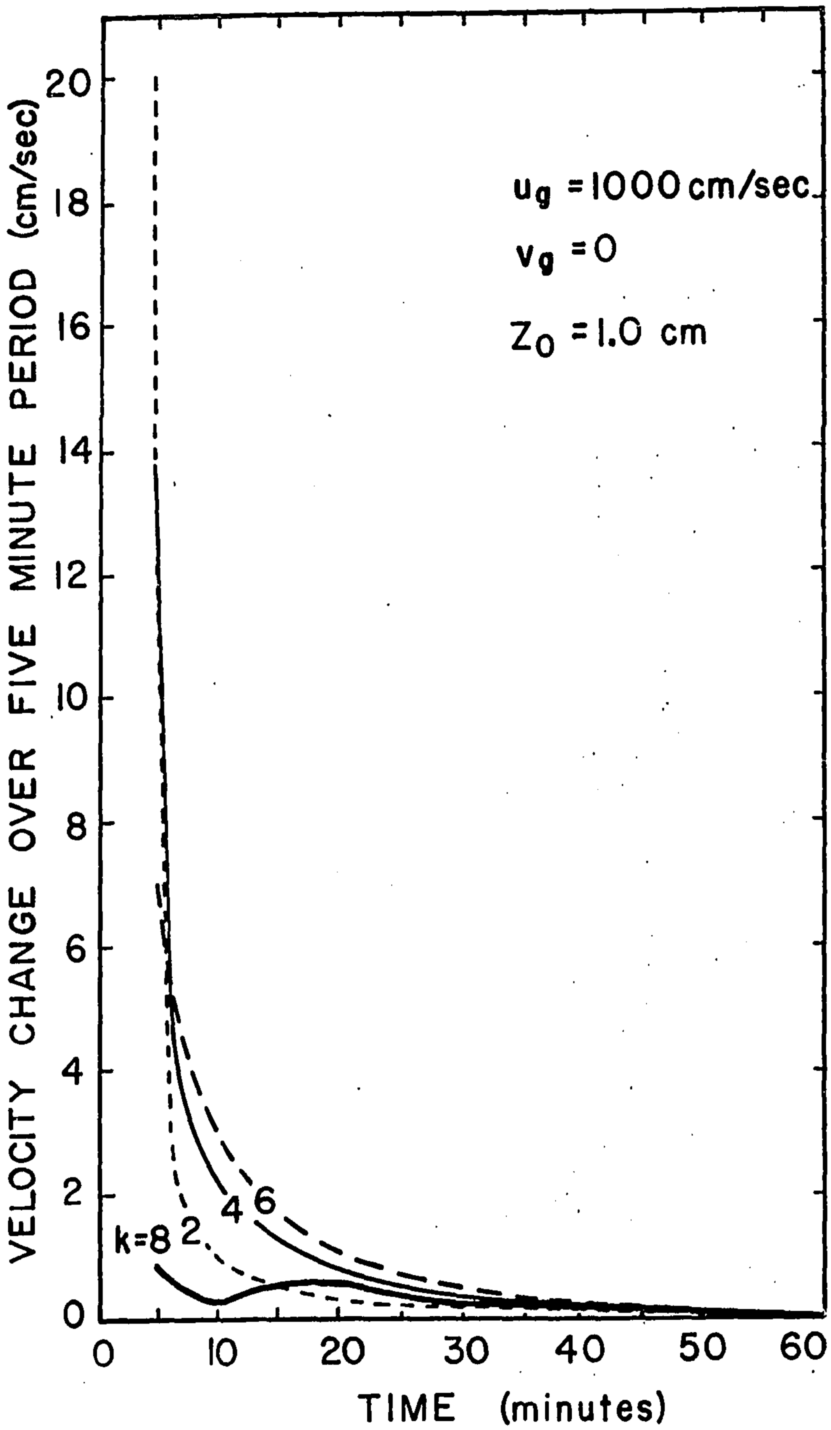

Fig. 5. Convergence of numerical solution for $K_z = k\, u_* \,(z + z_0)$ as shown by change in the x-component velocity with time at various grid heights k.

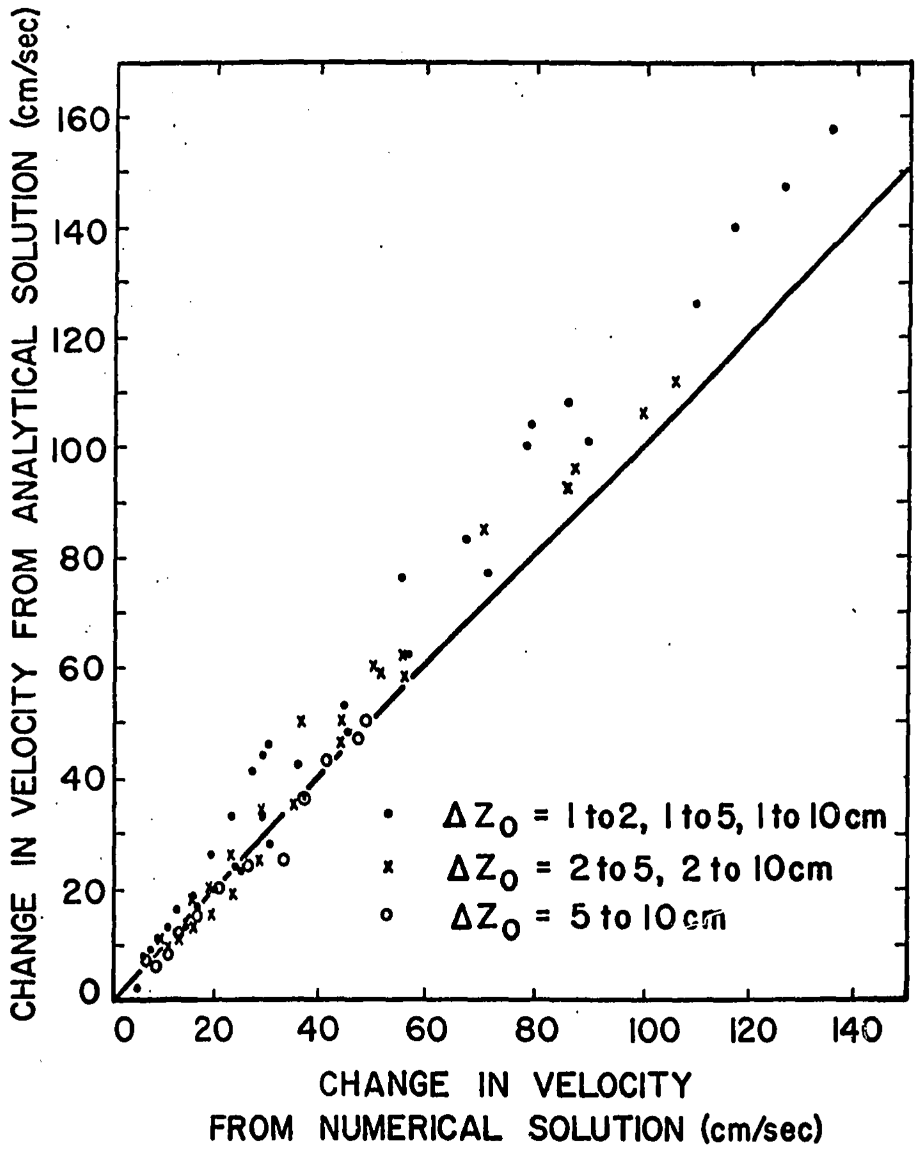

Fig. 6. Scatter diagram of velocity change due to change in roughness parameter for analytical and numerical solutions for $K_z = k\ u_*$ $(z + z_o)$.

by Mapanao (1966). Results for $u_g = 1000$ cm/sec , $v_g = 0$, $f = 10^{-4}$ sec^{-1} , an adiabatic, barotropic atmosphere and $z_o = 1$ and 10 cm are shown in Figure 7 by the solid lines. Our numerical solutions use Mapanao's values as initial input; the results after integrating (3.21) and (3.22) for one hour are seen to agree with the initial input in much the same way as the preceding solutions involving Hankel functions. The general shape of the profiles is duplicated very well and both the actual values of velocity and the change in velocity resulting from changing roughness is reproduced reasonably well.

The friction velocity and surface cross-isobar wind angle are shown in Figures 8 and 9. The curves in both of these figures are taken from Blackadar (1962). The friction velocity for the Hankel function solutions is obtained from (6.18). For the numerical solutions it is computed from the wind profile between the first and second grid points above the surface. We can anticipate good agreement since we know the friction velocity is related to the slope of the wind versus height, and from previous figures we have already seen that the slope predicted by theory is duplicated quite well by the numerical solution. In fact, essentially the same value for friction velocity is obtained by using any combination of the first five grid points above the surface. Since, for a given roughness, the total discretization error for each of the lower grid points is about the same, there is little error in the slope. Only if we use the surface value of $u = v = 0$, which has no error associated with it, do we encounter a change in slope, hence

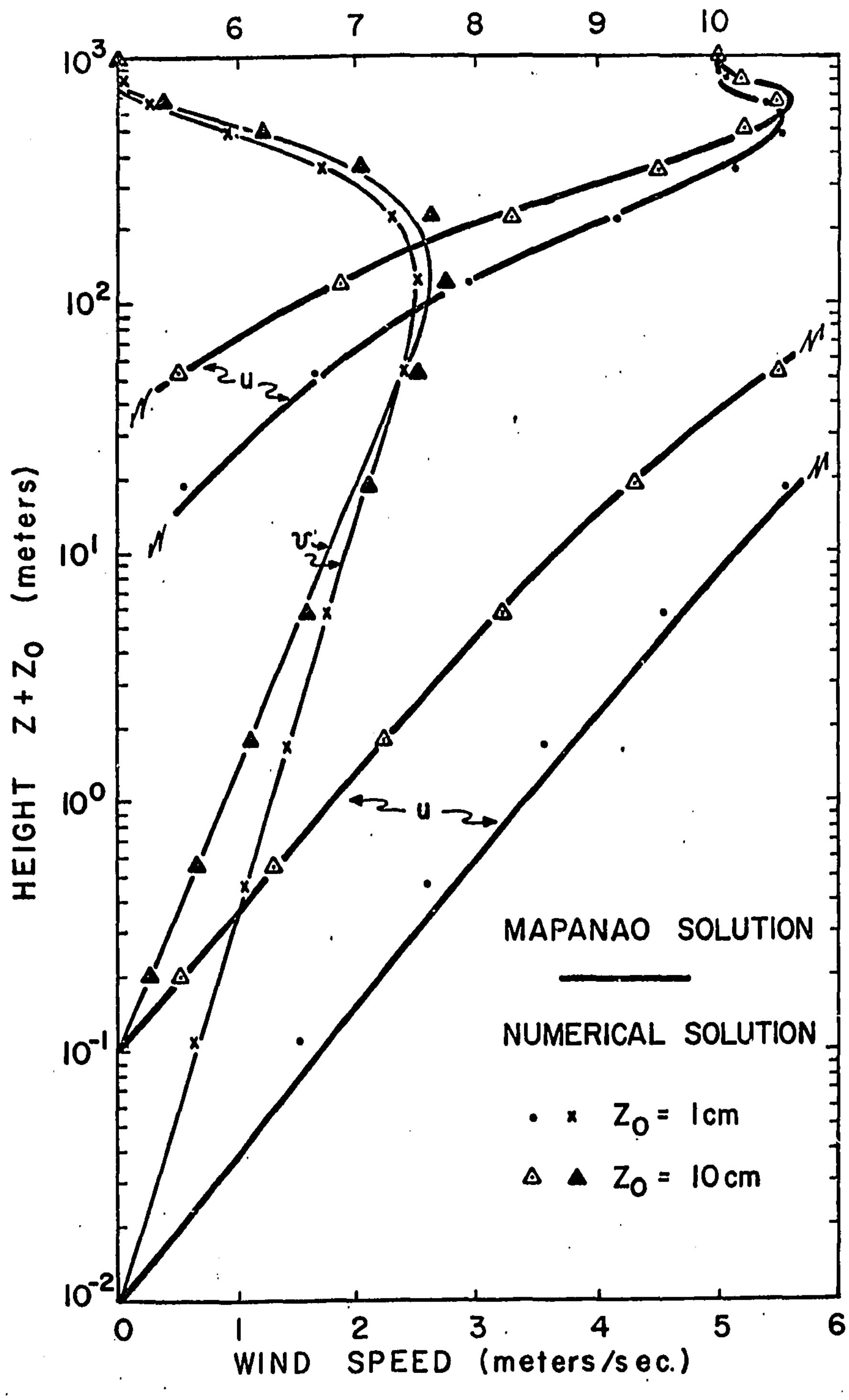

Fig. 7. Comparison of numerical solutions with solutions obtained by Mapanao for Blackadar's K_z distribution, U_g = 1000 cm/sec and roughness parameters of 1 and 10 cm.

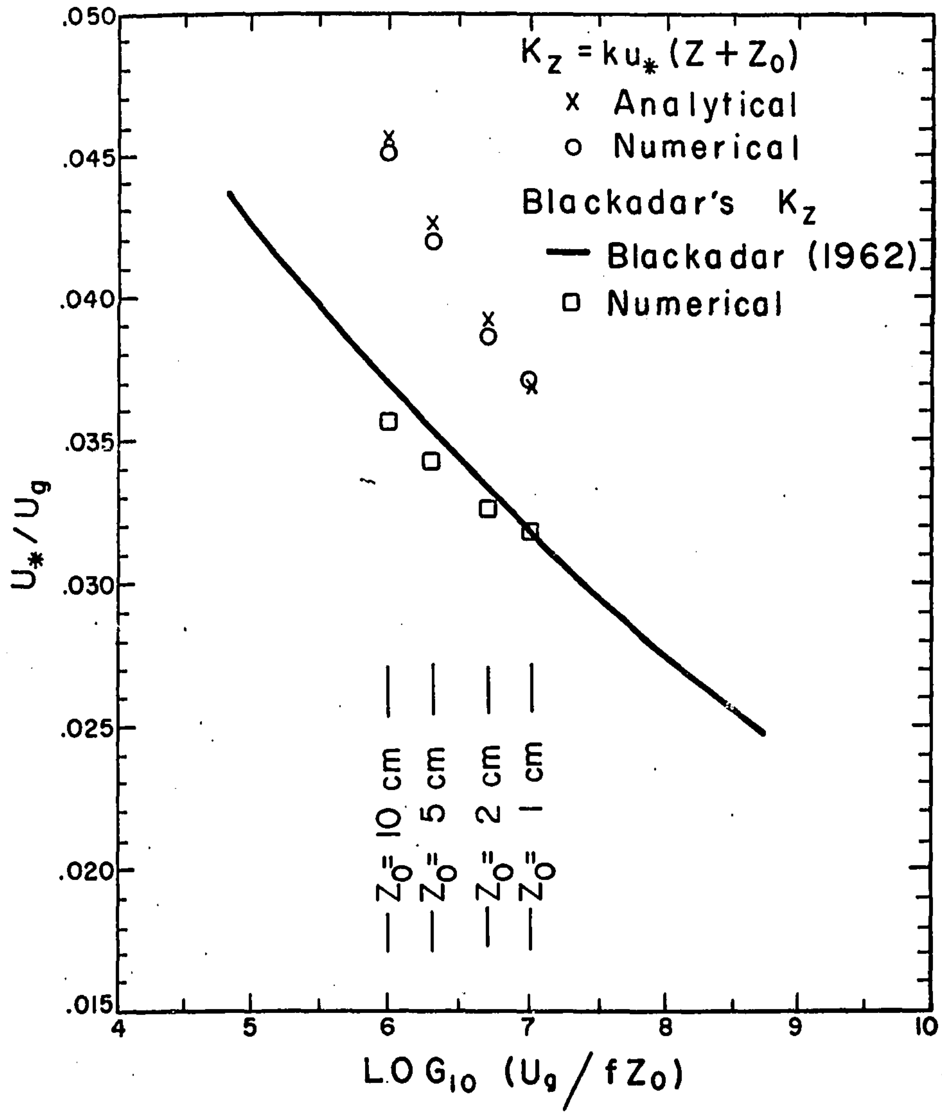

Fig. 8. Comparison of analytical and numerical determinations of friction velocity for various roughness parameters with U_g = 1000 cm/sec and $f = 10^{-4}\ sec^{-1}$.

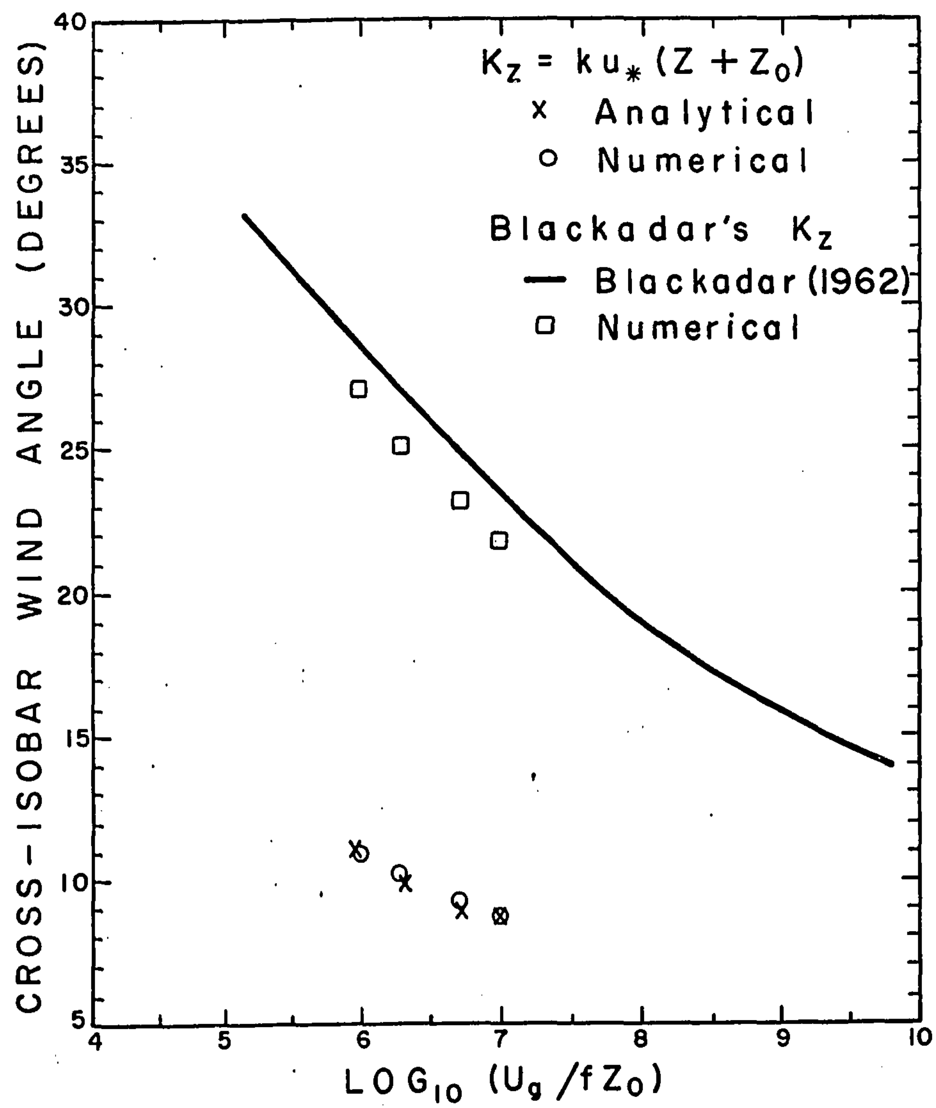

Fig. 9. Comparison of analytical and numerical determinations of cross-isobar wind angle for various roughness parameters with U_g = 1000 cm/sec and f = 10^{-4} sec^{-1}.

change in friction velocity and the associated surface stress. Because of the direction of the truncation error we are led to an overestimate of the slope, hence an underestimate of the friction velocity when using the surface grid point. The amount of underestimate decreases with increasing surface roughness, a result consistent with earlier statements concerning errors in the determination of the wind velocity.

The cross-isobar angle made by the surface wind is shown to be reproduced very well by the numerical solutions in Figure 9. Both the magnitude and variation of the values for different roughness conditions show excellent agreement.

All of the numerical results obtained in this chapter are for horizontally homogeneous conditions. For this condition, reasonably good agreement between analytical and numerical solutions was found when a small grid spacing in the lower levels was used. The author knows of no analytical solutions for a horizontally inhomogeneous lower boundary, hence a comparison with numerical solutions for this case is not possible. It is anticipated that, because of the considerably smaller magnitudes of the horizontal velocity gradients (as shown in the next section) as compared with the vertical gradients, the inclusion of a discontinuity in roughness parameter would not significantly alter the conclusions of this chapter. It seems reasonable to assume that the computational errors associated with the finite difference approximation as determined from the preceding analysis for horizontally homogeneous conditions will be of the same magnitude for non-homogeneous conditions.

VII. COMPUTATIONAL RESULTS FOR TWO-DIMENSIONAL FLOW OVER INHOMOGENEOUS TERRAIN

The two-dimensional distributions of horizontal velocity, vertical velocity and eddy shearing stress were determined by solving the finite-difference analogs to equations (3.6) through (3.9) on a 14 by 25 grid. The vertical and horizontal grid spacings are shown in Table I, and were computed from equations (3.1) and (3.2) with $a_1 = 2.0$, $a_2 = 771.0$, $b_1 = 0.8$, $b_2 = 4.0$ and $b_3 = 0.00005$. Component geostrophic wind velocities of $u_g = 1000$ cm/sec and $v_g = 0$ were used along with a constant potential temperature of 300°K throughout the grid array and a pressure of 900 mb along the upper boundary. On the lower boundary $u = v = w = 0$ and along the upper boundary, $u = u_g$ and $v = w = 0$. Lateral boundary conditions were $w = 0$ and no horizontal gradients of the horizontal velocities.

Computations were performed for the following roughness changes: (a) 1 to 10 cm, (b) 5 to 1 cm, (c) 2 to 1 cm, (d) 1 to 2 cm, and (e) 1 to 7.39 cm. One value of the roughness parameter was assigned to j values from one through twelve and the other to j equal thirteen through twenty-five. Initial conditions for the velocity components were obtained by integrating an equivalent set of equations for horizontally homogeneous conditions for one hour. These simpler equations used Mapanao's solutions for starting values as described in the preceding chapter. The results for various roughness parameter values are shown in Table II.

TABLE I. HEIGHT ABOVE THE ZERO-VELOCITY LEVEL FOR THE HEIGHT INDEX k, AND DISTANCE FROM THE ROUGHNESS DISCONTINUITY FOR THE HORIZONTAL INDEX j.

k	z (meters)	j	x (meters)	j	x (meters)
1	0.0	1	-3100.	13	2.5
2	0.0995	2	-1877.	14	7.5
3	0.446	3	-1135.	15	15.8
4	1.643	4	- 684.	16	29.3
5	5.689	5	- 411.	17	51.8
6	18.43	6	- 245.	18	88.7
7	52.16	7	- 144.6	19	149.6
8	119.6	8	- 83.7	20	250.1
9	221.1	9	- 46.8	21	416.
10	348.4	10	- 24.3	22	689.
11	492.9	11	- 10.7	23	1140.
12	648.9	12	- 2.5	24	1882.
13	812.9			25	3105.
14	982.5				

TABLE II. HORIZONTAL VELOCITY COMPONENTS WHICH WERE USED AS INITIAL CONDITIONS FOR THE TWO-DIMENSIONAL NUMERICAL MODEL COMPUTATIONS.

k	z_o = 1 cm (cm/sec)		z_o = 2 cm (cm/sec)		z_o = 5 cm (cm/sec)		z_o = 10 cm (cm/sec)	
1	0.0	0.0	0.0	0.0	0.0	0.0	0.0	0.0
2	155.3	61.9	127.8	54.5	84.8	39.6	54.2	27.7
3	260.5	103.7	229.4	97.6	177.7	82.7	133.8	68.2
4	357.4	141.7	325.9	138.2	273.6	126.8	226.3	114.8
5	453.8	178.3	422.6	177.6	372.1	170.9	324.9	163.2
6	554.8	213.1	524.4	215.4	476.6	213.8	430.8	211.1
7	667.5	242.4	638.4	247.7	594.2	251.6	550.7	254.4
8	794.4	254.2	767.4	262.2	728.5	271.3	688.9	279.5
9	919.3	232.2	896.2	241.3	864.5	254.2	830.8	265.8
10	1013.5	172.8	996.8	181.5	974.5	195.3	949.0	207.7
11	1053.6	93.6	1047.8	100.2	1037.6	112.1	1023.5	123.1
12	1039.2	28.4	1045.4	28.3	1048.0	34.3	1047.7	40.7
13	1005.7	2.3	1010.3	1.3	1015.6	0.1	1020.7	- 1.0
14	1000.0	0.0	1000.0	0.0	1000.0	0.0	1000.0	0.0

In section A of this chapter, case (a) is used to determine the relative order of magnitude of the various terms in the equations. The computational results for cases (b), (c) and (d) are presented in detail in section B, while in section C, case (e) is used to compare our results with those of Panofsky and Townsend (1964).

A. Evaluation of Individual Terms

In Chapter VI, it was found that in order to keep the truncation error within acceptable limits we must have a rather small grid spacing in the vertical near the lower boundary of the region of integration. The results of the stability analysis in Chapter IV showed that small grid spacing generally necessitates small time stepping in order to maintain computational stability. It becomes pertinent, then, not only because of scientific relevance, but also because of computer economics, to investigate the order of magnitude of the various terms in equations (3.6), (3.7), and (3.8) before any extensive computations are performed. In particular, we shall examine the horizontal eddy diffusivity term which appears in (3.6) and (3.7), and the terms involving the density which are present in (3.8). The relative mangitudes of these terms are determined by solving the finite-difference analogs to equations (3.6) through (3.9) for a roughness change from 1 cm to 10 cm.

The importance of the horizontal eddy diffusivity term was evaluated by performing computations for the three cases $K_x = 0$, $K_x = K_z$, and $K_x = 5K_z$. Comparison of the velocity fields for the two extreme cases showed a maximum difference in horizontal velocity of less than 1 cm/sec. This difference is very small when compared to the magnitude of the velocities as shown in Table II. Maximum vertical velocities differed by approximately ten percent; however, the basic pattern of vertical motion was unchanged. It would appear that our computational results are not significantly affected by the horizontal eddy diffusivity term, hence, it will be eliminated from the computations presented in the remainder of this paper.

Evaluation of the terms in the vertical velocity equation (2.16) show that the terms involving the second derivative of w and the cross-derivative of u are at least two to three orders of magnitude greater than any of the remaining terms. It was also found that these smaller terms have varying algebraic signs, and hence, exhibit a decided tendency to cancel one another. We are thus led, numerically, to conclude that adequate computational accuracy should be obtained by considering the decidedly simpler equation:

$$\frac{\partial^2 w}{\partial z^2} = - \frac{\partial^2 u}{\partial z \, \partial x}$$

which is recognized as the derivative with respect to z of the equation of continuity for two-dimensional, incompressible flow. That this equation should be adequate for describing most atmospheric flow has also been shown by Prandtl and Tietjens ((1934), pp. 224-232).

The computational results which are to be presented in the remainder of this paper will be obtained from equation (3.21) and (3.22) with the frictional terms given by the vertical eddy viscosity terms only, and a simplified version of (3.23) which appears as:

$$(7.1) \qquad \left[\frac{1}{4}\left(\frac{b_5}{b_4^2} - 2.\right) w\right]_{j\,k+1} + w_{jk} - \left[\frac{1}{4}\left(\frac{b_5}{b_4^2} + 2.\right) w\right]_{j\,k-1}$$

$$= \frac{1}{8}\left(\frac{a_3}{b_4}\right)_{jk} \left(u_{j+1\,k+1} + u_{j-1\,k-1} - u_{j+1\,k-1} - u_{j-1\,k+1}\right)$$

B. Computed Fields of Velocity and Eddy Shearing Stress

As air passes over a discontinuity in surface roughness, one would intuitively expect to first notice reactions to this change in the lowest layers, with progressive changes at higher levels as the entire atmospheric boundary layer eventually readjusts to new equilibrium conditions. Our intuition is substantiated by Figure 10 where the solid curves represent the change in cm/sec in the magnitude of the horizontal velocity vector associated with a change in the roughness parameter from 5 to 1 cm. The dot-dash curve in Figure 10 represents the location where the velocity has increased by two-tenths of one percent over the upstream equilibrium value. It is seen that a change in the horizontal velocity takes place upstream from the roughness discontinuity. In the lower levels the curve representing $(\Delta V/V) = 0.002$ is nearly ten meters upwind

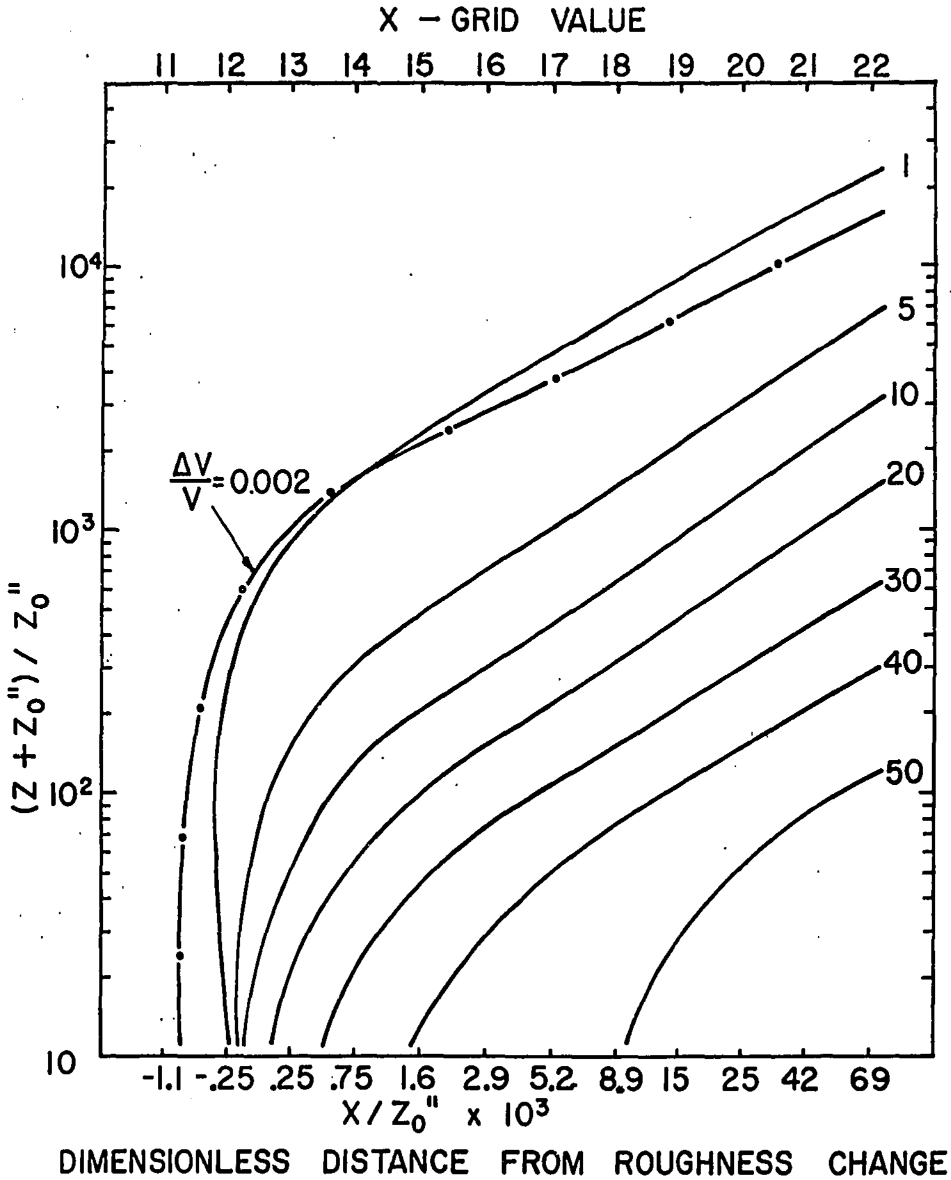

Fig. 10. Increase in horizontal velocity in cm/sec associated with a roughness change from 5 to 1 cm with U_g = 1000 cm/sec.

from the discontinuity for the case shown in Figure 10. Similar upwind effects have been measured in field observations by Stearns and Lettau (1963).

Once the change in the horizontal velocity has been determined from the prognostic equations (3.21) and (3.22), the vertical velocity can be calculated from the diagnostic equation (7.1). Figure 11 shows the vertical motion associated with the change in horizontal velocity depicted in Figure 10. The maximum downward velocity of 6.7 cm/sec is located above the thirteenth horizontal grid point (2.5 meters downstream from the discontinuity) and the eighth vertical grid point (120 meter height). Downward motion continues to persist downstream from the change in roughness, but the magnitude of the vertical velocity decreases markedly as we move away from the immediate vicinity of the discontinuity. It is interesting to note that there is a definite upstream effect on the vertical velocity, a factor directly related to the upstream changes in the horizontal velocity mentioned earlier. In addition, there exists in the lower levels and downstream from the discontinuity, a region where the vertical motion has practically vanished. This region of negligibly small vertical motion is increasing in depth with increasing distance from the discontinuity.

The eddy shearing stress was discussed briefly in Chapter II. The component stresses which arise from the vertical variation of the horizontal wind were written as

$$(7.2) \quad \tau_{xz} = -\rho\overline{u'w'} = K_z\rho\frac{\partial u}{\partial z} \quad ; \quad \tau_{yz} = -\rho\overline{v'w'} = K_z\rho\frac{\partial v}{\partial z}$$

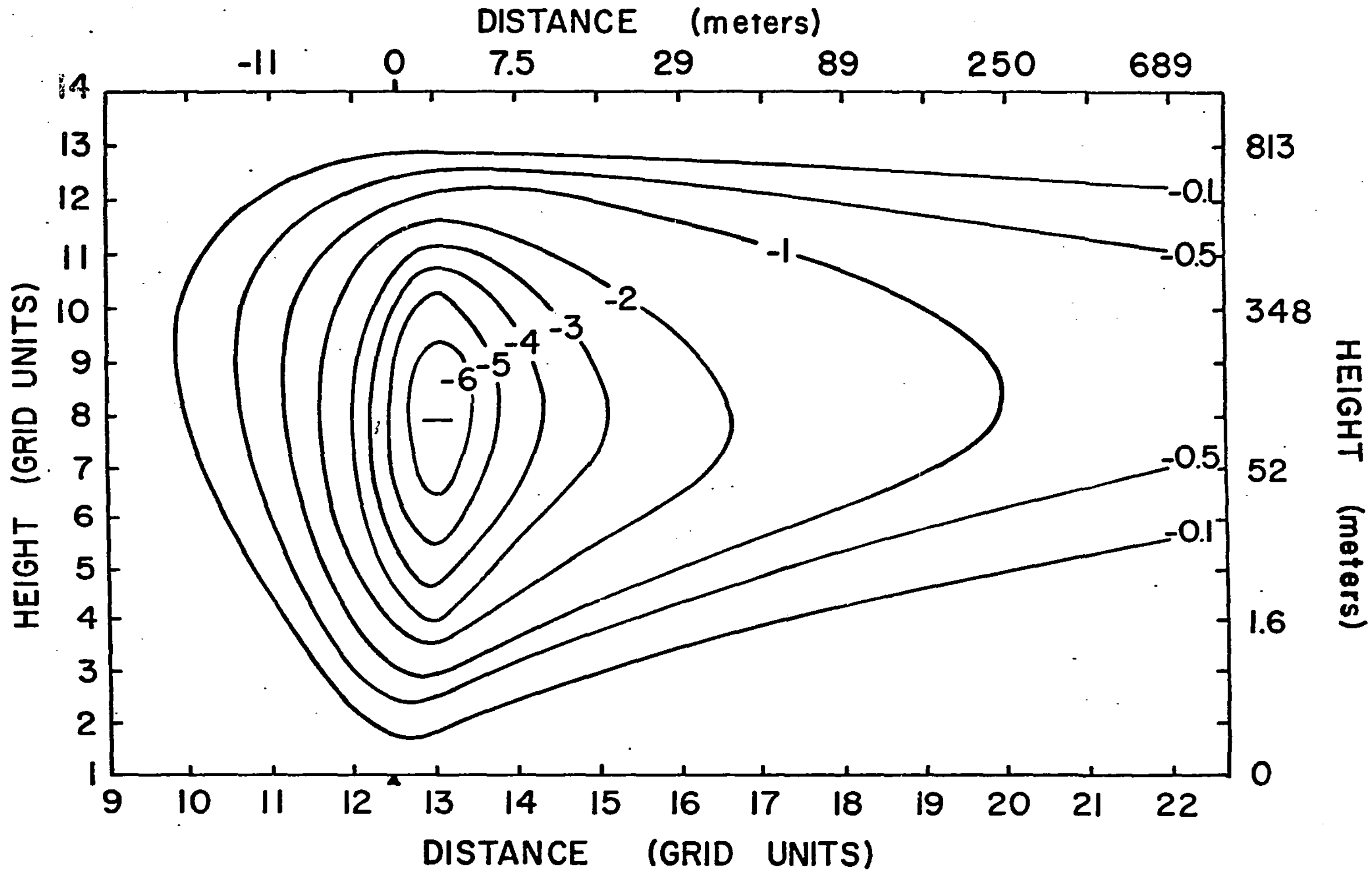

Fig. 11. Vertical velocity in cm/sec associated with a roughness change from 5 to 1 cm with U_g = 1000 cm/sec and $f = 10^{-4}$ sec^{-1}.

with the total eddy shearing stress being the vector sum of these two components. It should be noted that the above eddy shearing stress represents the flux of momentum across a horizontal plane due to velocity fluctuations (Sutton (1953), pp. 65).

Because the earth's surface is not horizontally homogeneous, except, occassionally, over large bodies of water, the flux of momentum from atmosphere to earth is not uniform. The boundary layer wind profile must repeatedly readjust to changing surface conditions. The effect of these horizontal inhomogeneities on field observation programs, local circulations, and the atmospheric energy balance was discussed in Chapter I. We are now in a position to examine the manner in which the momentum flux varies as a result of a change in surface roughness, and the time (or distance) required for new equilibrium conditions to be established.

The results obtained by computing the stress vector from the components given in equation (7.2) for a roughness change from 5 to 1 cm are shown in Figure 12. The curves representing upstream and downstream equilibrium, steady state conditions are labeled with $-\infty$ and $+\infty$, respectively. Other curves are labeled with j values and correspond to downwind distances of 2.5, 15.8, 51.8, and 416 meters from the discontinuity for j equal to 13, 15, 17, and 21, respectively (see Table I).

Consideration of equations (7.2), (2.19), and (2.20) shows that the eddy stress is a function of surface roughness and vertical shear of the horizontal wind. For flow from rough to smooth terrain, the change in surface roughness would decrease the eddy stress. In

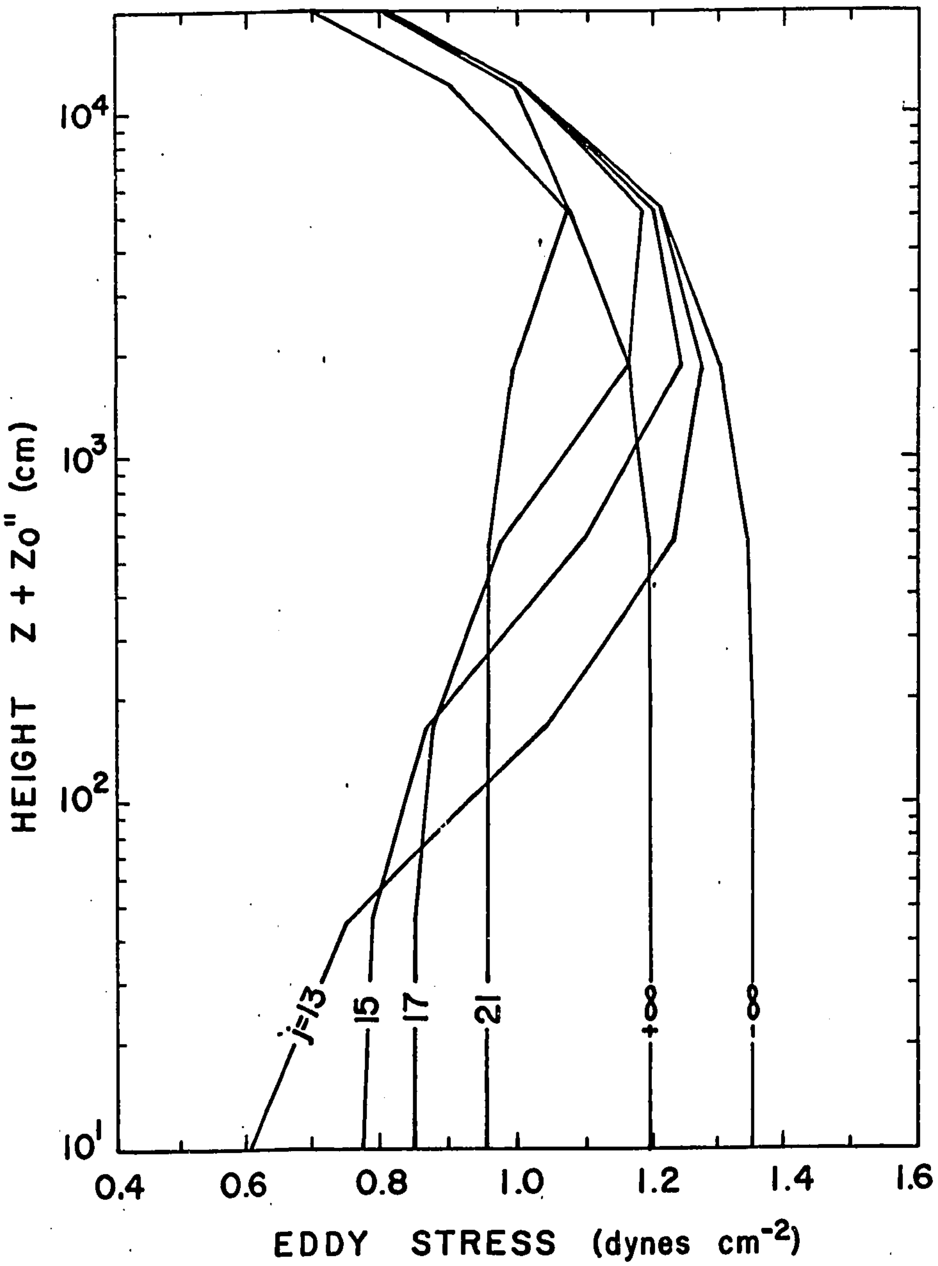

Fig. 12. Vertical and horizontal variation of eddy stress associated with a roughness change from 5 to 1 cm.

the lower layers it is apparent from Figure 7 that the equilibrium velocity shear is smaller over a rough surface than over a smooth surface. We have already seen from Figure 10 that the horizontal velocity approaches the new equilibrium value monotonically. Hence, for flow from rough to smooth terrain the low level velocity shear will be much too small near the discontinuity, and will increase monotonically downstream as the velocity approaches new equilibrium flow conditions over the smoother surface.

These expectations are verified when we examine Figure 12. The character of the low level momentum flux changes markedly when the change in roughness is encountered. Instead of balanced flow with constant eddy stress in the lower layers, we find the momentum flux increasing with height for $j = 13$. This implies convergence of the downward flux of horizontal momentum, and, in order for the total momentum to be conserved, results in increasing horizontal velocities. The velocity increase has already been shown in Figure 10. In order to have conservation of mass, the horizontal accelerations are accompanied by downward motion as shown in Figure 11. The vertical motion thus contributes to the downward flux of horizontal momentum and the reestablishment of equilibrium flow conditions.

The remaining curves in Figure 12 show that a logarithmic wind profile (characterized by constant eddy stress) is gradually established in the lower portions of the boundary layer. This corresponds very closely to the region shown in Figure 11 where the magnitude of the vertical velocity becomes less than 0.1 cm/sec. The ratio of the height to downwind distance from the discontinuity for this region is between 1/50 and 1/100. It appears that a fetch of considerable extent is necessary before complete equilibrium is achieved. Extrapolation of the eddy stress as computed for the lowest layer suggests a fetch of at least five kilometers in order to reach ninety percent of the final equilibrium value. It is rarely possible to satisfy such an upwind fetch requirement in the atmosphere, hence we might conclude that many low level wind profile observations are taken under quasi-equilibrium conditions. The observed profile may be logarithmic, but the eddy shearing stress (or friction velocity) might not yet have reached its equilibrium value.

Two additonal examples of the computed field of vertical motion are shown in Figure 13. In this figure, the dashed lines are associated with the downward motion which results from a roughness change from 2 to 1 cm while the solid lines correspond to the upward motion resulting from a roughness change from 1 to 2 cm. The magnitude of the maximum value of the vertical motion is approximately 2.2 cm/sec in both cases. The horizontal position of the maximum is the same as in the preceding 5 to 1 cm roughness case, but the height is near 52 meters, which is one grid distance below the preceding case.

The main difference between the dashed and solid curves is the slightly smaller absolute values associated with the downward motion at low levels near the discontinuity. This difference appears to be attributable to the manner in which the shear of the horizontal

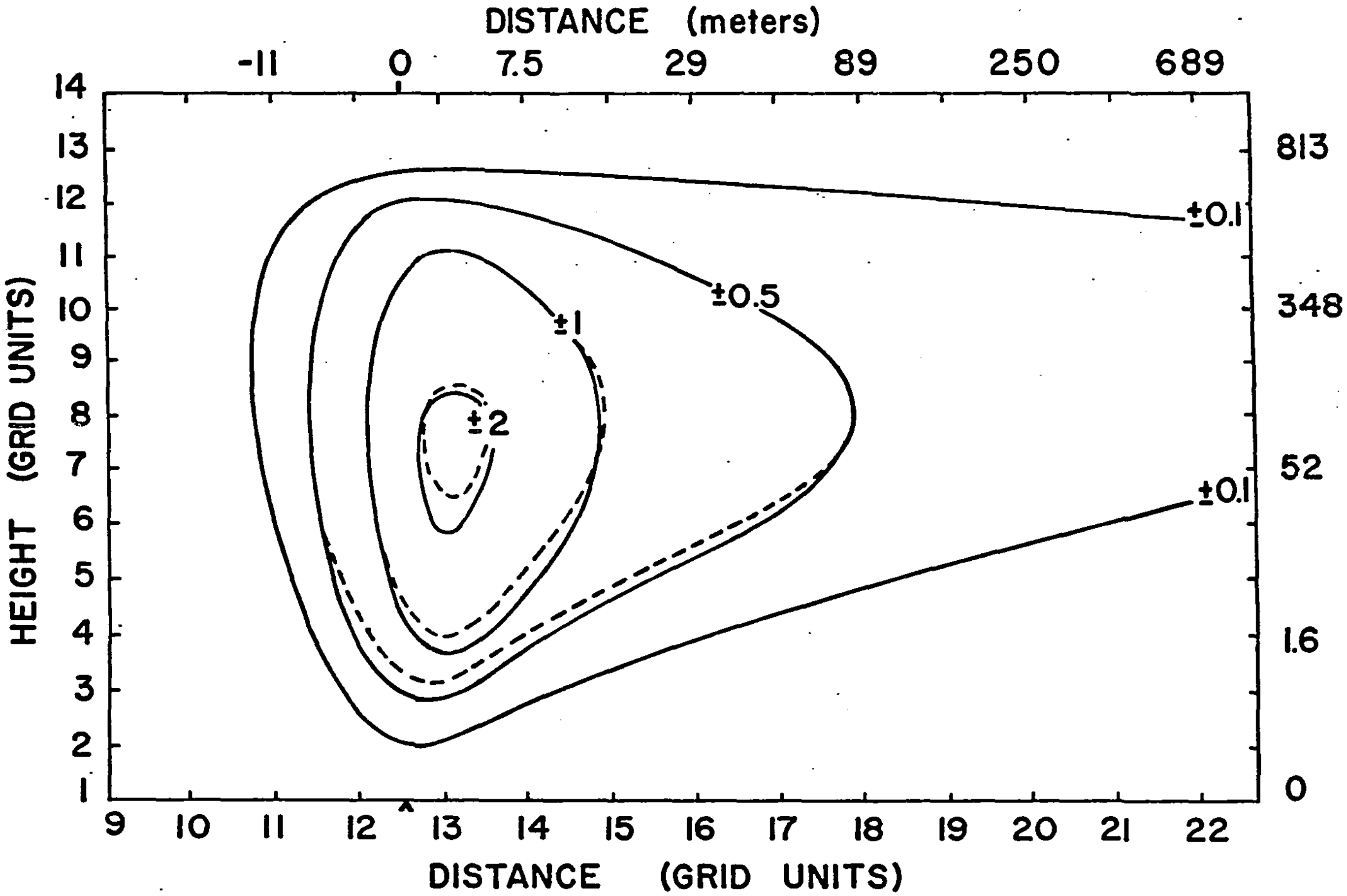

Fig. 13. Vertical velocity in cm/sec associated with a roughness change from 1 to 2 cm (solid) and 2 to 1 cm (dashed) with U_g = 1000 cm/sec and f = 10^{-4} sec^{-1}. Negative values are associated with decreasing roughness and positive values with increasing roughness downwind.

velocity changes in these two cases, and the resulting effect of the velocity shear on the eddy diffusivity (see equation (2.19)). As we pass from smooth to rough terrain, the velocity shear becomes extremely large, resulting in an excessively large eddy stress near the lower boundary. The resulting effect on the horizontal velocity is to slow it down rapidly resulting in large positive vertical motion. For flow from rough to smooth terrain, the shear and stress are smaller, resulting in comparatively slower changes in the horizontal velocity and somewhat smaller vertical velocities.

The variation of eddy shearing stress for roughness changes from 2 to 1 cm and 1 to 2 cm is shown in Figures 14 and 15, respectively. The main point of interest in these figures is that flow from smooth to rough terrain results in an approximately twenty percent larger change in surface stress than the same change from rough to smooth terrain. Since the magnitude of the roughness change is the same, the explanation must lie in the differing character of the wind shear for the two cases. For the type of flow considered, the wind shear can cause the surface stress to become extremely large for flow from smooth to rough terrain. On the other hand, flow from a rough to a smooth surface is associated with a stress which has a bounded minimum value of zero. Over any finite interval this results in a somewhat larger change in stress for flow from smooth to rough terrain, as compared with rough to smooth flow. It is, in fact, a type of hysteresis effect which would result in a larger net momentum flux than one might expect from a simple examination of surface terrain.

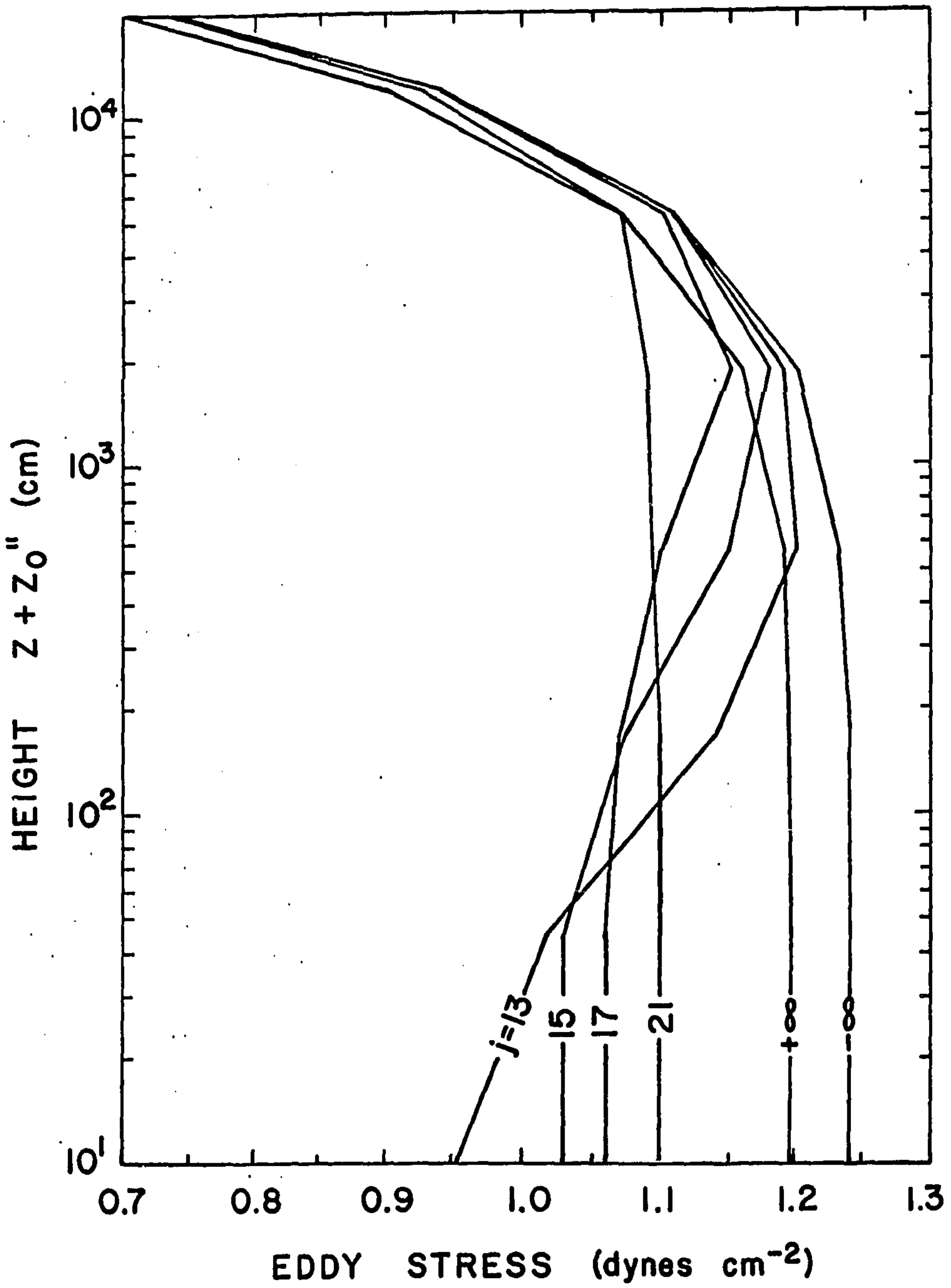

Fig. 14. Vertical and horizontal variation of eddy stress associated with a roughness change from 2 to 1 cm.

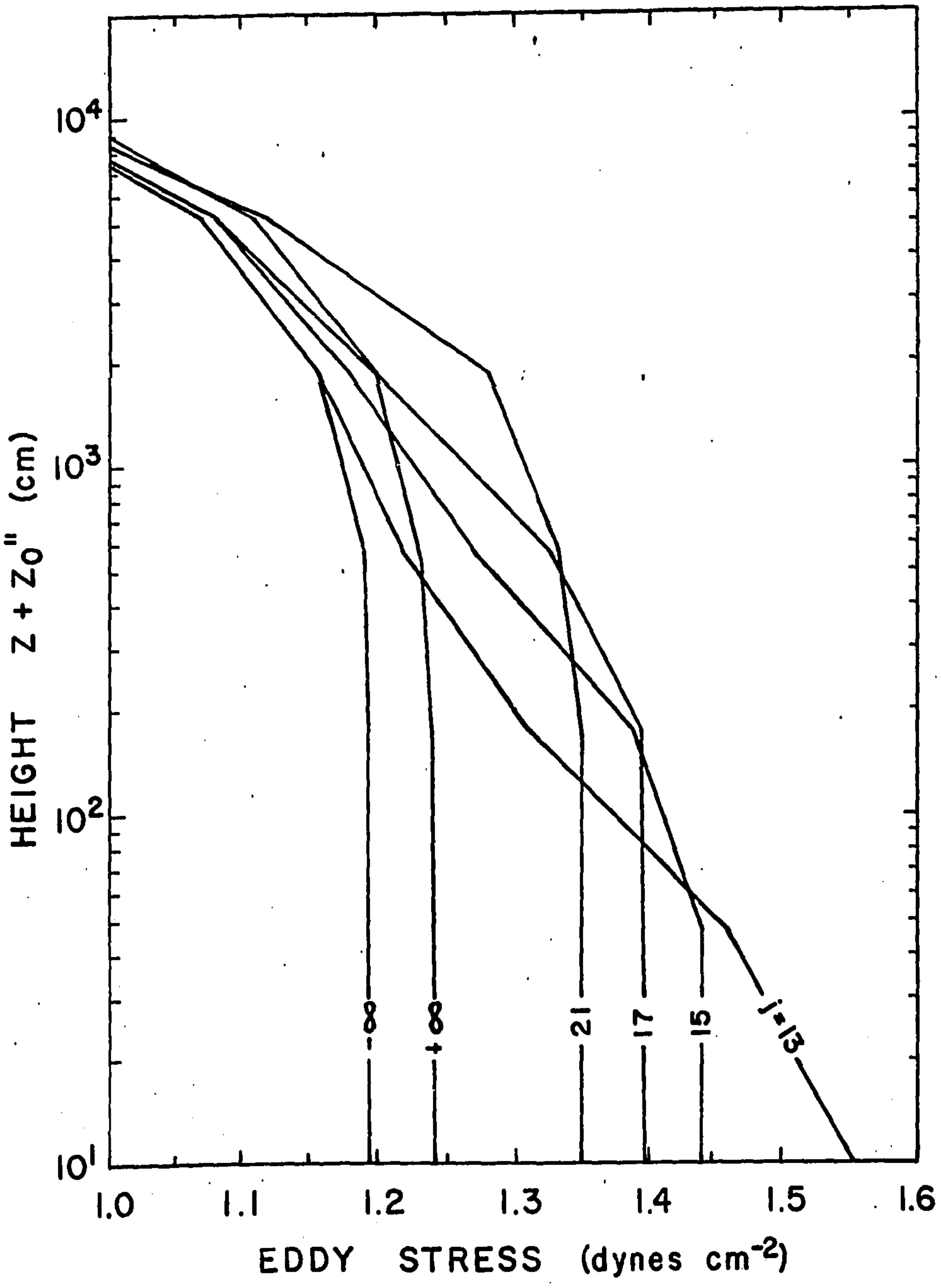

Fig. 15. Vertical and horizontal variation of eddy stress associated with a roughness change from 1 to 2 cm.

C. Comparison with Other Studies

Panofsky and Townsend (1964), in an extension of Elliott's (1958) work, employ classical boundary layer techniques to study the downwind variation in height of an interface (or zone) which separates flow in equilibrium with the upwind surface roughness from that approaching equilibrium with the downwind roughness. By neglecting the coriolis term and assuming incompressible flow, no net vertical displacement of the streamlines downwind of the discontinuity, and linear variation with height of the friction velocity such that no discontinuity in stress occurs at the interface, Panofsky and Townsend derive an expression for interface height as a function of downwind distance for various roughness changes. Results for three particular values of roughness change as presented in their article are shown by dashed lines in Figure 16. In this and the next figure, z_o' is the upstream and z_o'' the downstream roughness parameter.

Some difficulty is encountered when we attempt to compare our results with those of Panofsky and Townsend. Because of the existence of vertical motions and the nature of our assumption concerning the step-change in mixing-length, the field of horizontal motion is modified to some extent throughout the boundary layer as soon as the change in roughness takes place. However, if we define a 0.2 percent change in the horizontal velocity vector as representing a significant change, then we obtain the curves shown as solid lines in Figure 16. These curves are obtained by analysis of the horizontal velocity fields associated with the roughness changes of 5 to 1 cm, 2 to 1 cm,

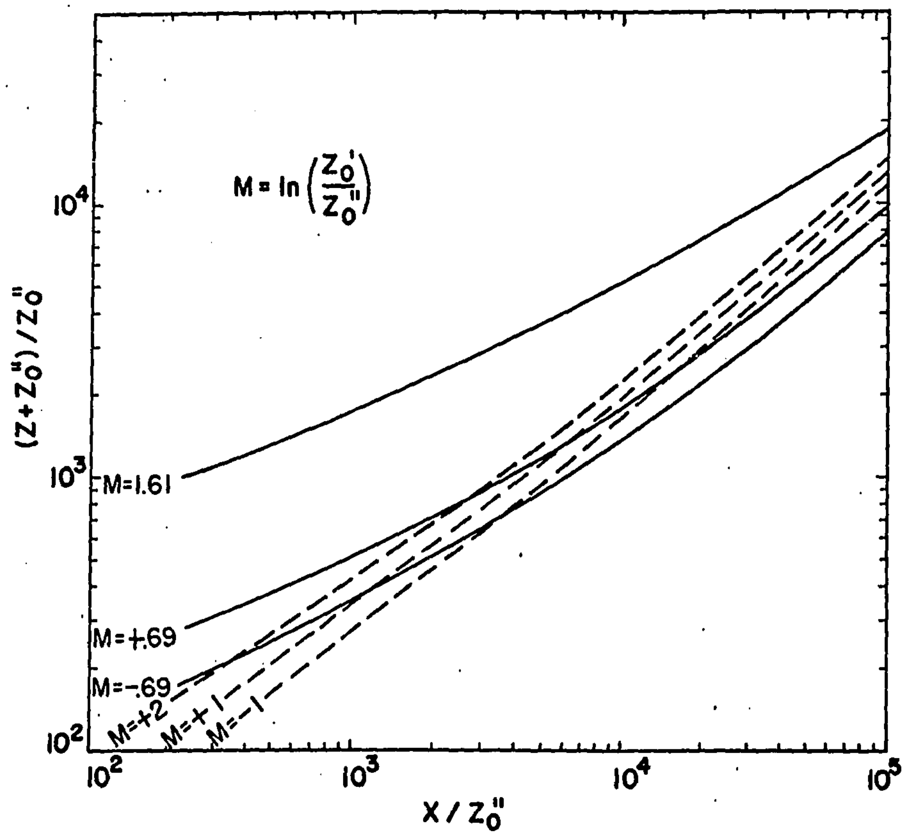

Fig. 16. Variation of height of interface with distance from the roughness discontinuity. Dashed lines are from Panofsky and Townsend (1964). Solid lines designate where change in velocity equals 0.2 percent of upstream value.

and 1 to 2 cm described in the preceding section of this chapter.

It is encouraging to note that the general tendency of both sets of curves is similar. Not only does the depth of the disturbed layer increase nearly linearly with distance downwind, but the depth at a given downwind distance increases as the logarithm of the ratio of the upwind to downwind roughness parameter increases (i.e., as we go from increasingly rough to smooth underlying terrain). Most of the apparent discrepancy between the two sets of curves in Figure 16 is probably related to the lack of uniqueness in the definition of the interface. However, for small x, some of the difference must also be related to the omission of any upstream effect by Panofsky and Townsend.

Figure 17 compares our computations of the downwind variation of the vertical profile of the horizontal wind with those of Panofsky and Townsend. The solid curves are taken from their article, the one labeled with $-\infty$ representing upstream equilibrium conditions. The downstream friction velocity is represented by u_*''. Solid dots represent results from our numerical computations for a roughness change from 1.0 to 7.39 cm. All other boundary conditions were the same in these computations as those used in the preceding section. Numerical agreement is seen to be remarkably good, giving further credence to our earlier speculation that the interface differences as shown in Figure 16 are related primarily to a matter of definition.

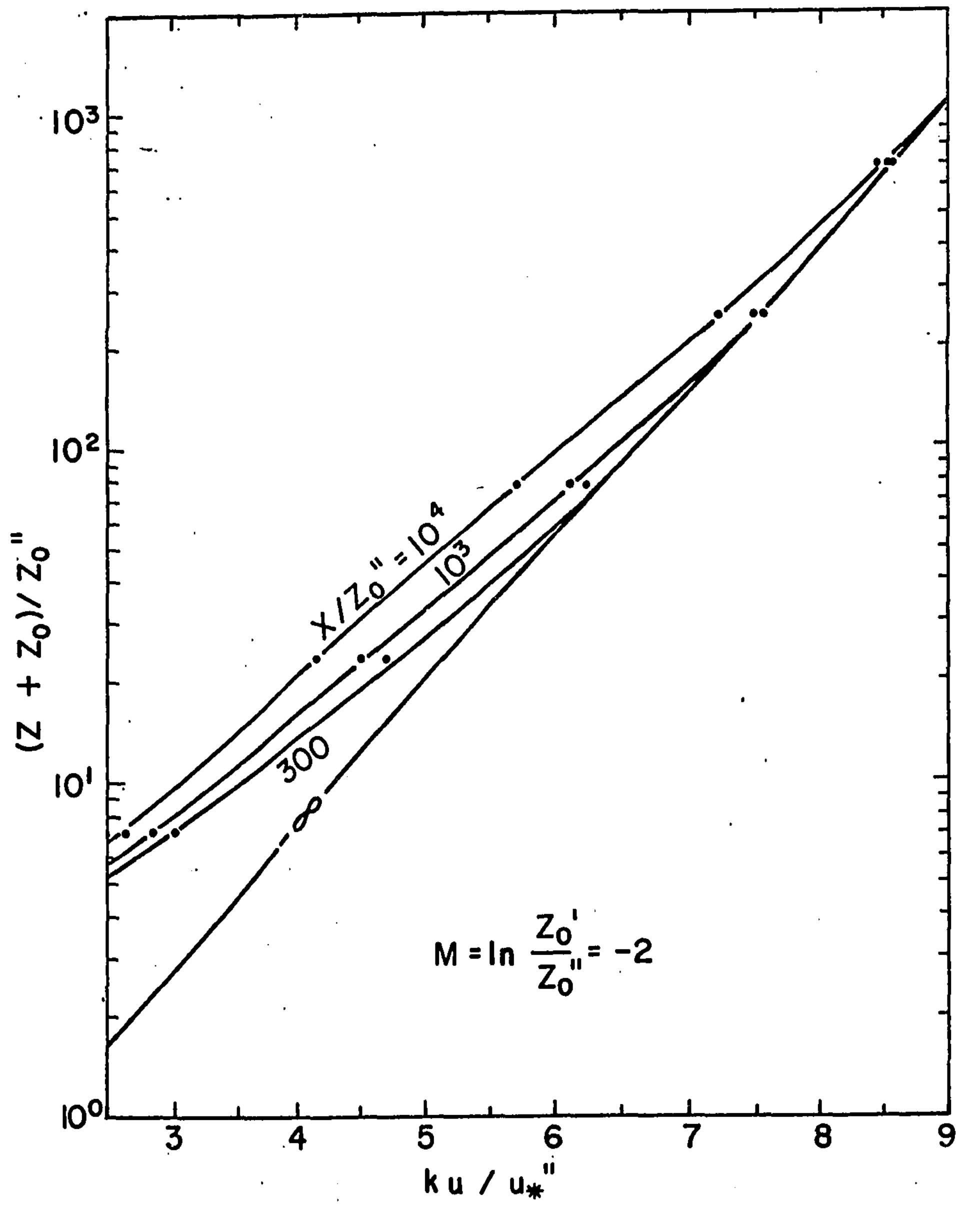

Fig. 17. Comparison of results of Panofsky and Townsend (solid lines) with numerical results for flow from smooth to rough terrain.

Onishi (1966) has written a computer program similar to ours, but for steady-state conditions. He also essentially duplicated these curves of Panofsky and Townsend. The only perceptible difference between their results was in the upper portion of each curve where Onishi's computations indicated a more asymptotic approach to upstream equilibrium conditions. Onishi has also considered a dynamic pressure force resulting from the sudden change in horizontal velocity near the roughness discontinuity. His results suggest that for large changes in roughness, the character of the air flow near the roughness change is horizontally smoothed by these local pressure gradients. This results in a larger upstream effect and smaller maximum vertical velocities. For the roughness and distance values which we are considering, this pressure force would be a second order effect. However, if one were to examine the air structure within a few tens of centimeters in the horizontal, such a pressure term would need to be retained in the governing equations. This effect could be particularly important if the height of the lower boundary changes at the discontinuity (i.e., zero-plane displacement).

Panofsky and Townsend used data obtained by the University of Wisconsin and reported by Kutzbach (1961) to show good agreement between their theory and observations. The conformity between our computations and the results of Panofsky and Townsend shown by Figure 17 would suggest that Kutzbach's observations would also agree with our results. Further quantitative comparison with available observations would be of questionable validity. Our numerical model is not sufficiently general to allow for zero-plane displacement and non-neutral atmospheric stability, both of which are probably significant and certainly present in the University of Wisconsin observations. However, Stearns and Lettau (1963) have computed the fields of vertical motion and eddy shearing stress from measured horizontal velocities for flow from ice to a Christmas tree forest. Their results show good qualitative agreement with our computations. More exact comparison will need to await further generalization of our numerical model, and more observations over a wider range of atmospheric conditions.

VIII. SUMMARY AND CONCLUSIONS

The fundamental purpose of this study was to formulate a two-dimensional, time dependent numerical model of the atmospheric boundary layer and to use this model to investigate various characteristics of air motion when a change occurs in the roughness of the underlying surface. The model assumes adiabatic stratification, dry adiabatic changes of state, no horizontal mixing, incompressible flow, no dynamic pressure effects due to flow accelerations and no vertical displacement of the zero-velocity level at the lower boundary when the roughness change occurs.

A computational stability analysis was made which provided the relationship between time-step and grid spacing which must be satisfied to obtain convergence of the numerical solution. For horizontally homogeneous conditions, comparison of the numerical solutions with various analytical solutions showed that the errors inherent in the finite difference formulation can be reduced to any desirable level by reducing the grid spacing, particularly near the lower boundary.

Computed quantities included the two-dimensional distribution of horizontal velocity, vertical velocity, and eddy shearing stress. Maximum vertical velocities were found above the discontinuity at a height on the order of 50 meters for a roughness change from 1 to 2 cm (and 2 to 1 cm) increasing to about 100 meters for a change from 5 to 1 cm. The magnitude of the vertical motion is approximately 2 cm/sec for the former and 7 cm/sec for the latter cases. Vertical velocities in excess of 0.1 cm/sec are found several meters upstream from the discontinuity and persist for several hundred meters downstream for the cases considered.

The computations also show that a nearly logarithmic wind profile with associated constant shearing stress becomes established throughout a layer of increasing depth as we move downstream from the roughness discontinuity. The ratio of the depth of this constant stress layer to the distance downwind from the discontinuity was found to be between 1/50 and 1/100. Reestablishment of the logarithmic profile does not imply equilibrium flow, however. Fetches on the order of several kilometers appear to be necessary before surface eddy stress values differ by less than ten percent from their final equilibrium values. The theoretical concept of equilibrium boundary layer flow probably rarely occurs in nature.

Quantitative comparison of our computations with Panofsky and Townsend (1964) showed excellent agreement. In addition, Panofsky and Townsend employed selected observational data of Kutzbach (1961) to show that their theory was consistent with observations. Lack of generality in our numerical model suggested that any further quantitative comparison with observations from the University of Wisconsin group would be of questionable validity. Of especial concern is our current inability to allow for zero-plane displacement and non-neutral atmospheric stability stratifications, both of which are probably significant and certainly present in the Wisconsin observations (see, for example, Stearns and Lettau (1963)). It should be noted, however, that the general features of the computed velocity and stress distributions agree very well with results presented by Stearns and Lettau, hence we at least have good qualitative agreement with observations.

In spite of the ability of the current numerical model to reproduce, both quantitatively or qualitatively, many of the observed features of air flow over a surface roughness discontinuity, it does possess several shortcomings. Perhaps most apparent is the lack of generality. Now that the basic theoretical framework has been established, only a moderate amount of additional work should be required to provide for zero-plane displacement, a large scale pressure gradient which varies with height, and some provision for non-neutral atmospheric stability stratifications. The resulting model could then more readily be compared with existing and future observational data.

Further investigation is also required to determine more explicitly the influence of local dynamically produced pressure gradients on the resulting airflow in the vicinity of discontinuities in the lower boundary. In addition, a search for numerical or mathematical techniques which would reduce the truncation error associated with the finite difference formulation might prove rewarding. It is anticipated that future research by the author and others will improve and extend the results of this study.

APPENDIX

Given below are the mathematical and physical quantities which were not defined explicitly in the text, or about which there may be some ambiguity. Notation derived from the English alphabet is presented first in alphabetical order, followed by Greek and mathematical symbols.

A	A constant of integration in chapter VI.
$A(z)$	A quantity which is a function of the coordinate z.
B	Represents the constant rate of change of eddy viscosity with height in chapter IV; a constant of integration in chapter VI.
c_p	Specific heat capacity of air at constant pressure.
d	Total differential operator.
$\underset{\sim}{g}$	Acceleration of gravity.
I	Identity (or unit) matrix.
i	Square root of minus one.
(i)	Used as a superscript to denote the ith eigenvalue.
j, k	Integer values used as subscripts to denote the finite difference grid position of the horizontal and vertical coordinates, respectively.
k	von Karman's constant (assumed equal to 0.4).
(lat)	Latitude.
m, n	Used to denote integer grid unit values of the horizontal and vertical coordinates respectively. Similar in meaning to the j, k subscripts above.

n	Used as a superscript to denote time step and confined to velocity components u and v plus equations (3.21) and (3.22).
p	Atmospheric pressure.
q	Heat (per unit mass).
R	Gas constant for dry air.
T	Temperature (in degrees Kelvin).
t	Time.
u, v, w	Velocity components in the x, y, and z directions, respectively.
u_g, v_g	Geostrophic velocity components in the x and y directions, respectively. Related to the large scale atmospheric pressure distribution by $u_g = -\frac{1}{\rho f}\cdot\frac{\partial p}{\partial y}$; $v_g = \frac{1}{\rho f}\cdot\frac{\partial p}{\partial x}$
$\bar{u}$	Mean, unperturbed velocity in the x direction.
u (x,z)	x-component velocity as a function of x and z coordinates.
u', w'	Eddy velocities (fluctuations from the mean) in the x and z directions, respectively.
u_a, u_n	x component velocities determined from analytical and numerical solutions, respectively.
V	Magnitude of the horizontal velocity vector.
x, y, z	In equations (2.1), (2.2), and (2.3) these are coordinate directions positive toward the east, north and upward, respectively. After two-dimensional assumption is made

(beginning with eq. (2.9) x may have any horizontal orientation.

z_o	Roughness parameter.
z_o', z_o''	Roughness parameter upstream and downstream from a roughness discontinuity, respectively.
α	A parameter used in chapter IV and defined by equation (4.14); also used in chapter VI to denote cross-isobar wind angle.
γ	A parameter used in chapter IV and defined by equation (4.14); also used in chapter VI to denote Euler's constant.
Δ	Finite difference operator.
Δz_o	Difference between two roughness parameter values.
$(\Delta z)_1$	Finite distance between lower boundary and first grid point in vertical direction.
$\lambda^{(i)}$	The ith eigenvalue.
λ	The limiting value for mixing-length at high elevations and defined by equation (2.21).
ρ	Atmospheric density.
τ_{12}	Eddy stress with first subscript denoting direction of stress and second subscript indicating plane (perpendicular to coordinate axis denoted by second subscript) on which stress is acting.
τ_o	Surface value of eddy shearing stress.
Ω	Angular velocity of the earth.
∂	Partial differential operator.

REFERENCES

Asai, T., 1965: "A Numerical Study of the Air-Mass Transformation over the Japan Sea in Winter", Journal of the Meteorological Society of Japan, Ser. II, Vol. 43, No. 1, pp. 1-15.

Blackadar, Alfred K., 1962: "The Vertical Distribution of Wind and Turbulent Exchange in a Neutral Atmosphere", Journal of Geophysical Research, Vol. 67, No. 8, pp. 3095-3102.

Brunt, D., 1920: "Internal Friction in the Atmosphere", Quarterly Journal of the Royal Meteorological Society, Vol. 46, No. 194, pp. 175-185.

Courant, R., K. Friedrichs and H. Lewy, 1928: Uber die Partiellen Differentialgleichungen der Mathematische Physik, Mathematische Annalen, Vol. 100, pp. 32-74. (Translation by W. L. Gates and M. H. Oberlander and issued as Sci. Rep. No. 2, Dynamical Weather Prediction Project, Dept. of Meteorology, UCLA, 18 Dec 1959).

Dobson, G. M. B., 1914: "Pilot Balloon Ascents at the Central Flying School, Upavon, during the year 1913", Quarterly Journal of the Royal Meteorological Society, Vol. 40, No. 170, pp. 123-135.

Ekman, V. Walfrid, 1905: "On the Influence of the Earth's Rotation on Ocean-currents," Arkiv for Matematik, Astronomi och Fysik, Band 2, No. 11, pp. 1-52.

Elliott, William P., 1958: "The Growth of the Atmospheric Internal Boundary Layer," Transactions of the American Geophysical Union, Vol. 39, No. 6, pp. 1048-1054.

Ellison, T. H., 1956: Atmosphere Turbulence, pp. 400-430 in Surveys in Mechanics, edited by G. K. Batchelor and R. M. Davies, Cambridge University Press, New York, 475 pp.

Estoque, M. A., 1962: The Sea Breeze as a Function of the Prevailing Synoptic Situation, Journal of the Atmospheric Sciences, Vol. 19, No. 3, pp. 244-250.

Forsythe, George E. and Wolfgang R. Wasow, 1960: Finite-Difference Methods for Partial Differential Equations, John Wiley and Sons, Inc., New York, 444 pp.

Frost, R., 1948: Atmospheric Turbulence, Quarterly Journal of the Royal Meteorological Society, Vol. 74, No. 321-322, pp. 316-338.

Holopainen, E. O., 1963: On the Dissipation of Kinetic Energy in the Atmosphere, Tellus, Vol. 15, No. 1, pp. 26-32.

Holopainen, E. O., 1964: Investigation of Friction and Diabatic Processes in the Atmosphere, Societas Scientiarum Fennica, Commentationes Physico-Mathematicae, XXIX 9, pp. 1-47.

Holzworth, George C., 1964: Estimates of Mean Maximum Mixing Depths in the Contiguous United States, Monthly Weather Review, Vol. 92, No. 5, pp. 235-242.

Jacobs, W., 1939: Unformung eines turbulenten Geschwindigkeits-profiles, Zeitschrift angewandte, Mathematik und Mechanik, Band 19, No. 2, pp. 87-100.

Jahnke, E. and F. Emde, 1945: Tables of Functions with Formulae and Curves, New York, Dover Publications, 382 pp.

Johnson, Warren B., 1965: Atmospheric Boundary-layer Dynamics over the Forests of Northeastern Wisconsin, pp. 45-145 in Studies of the Effects of Variations in Boundary Conditions on the Atmospheric Boundary Layer, Final report from the Department of Meteorology, University of Wisconsin to Department of Meteorology, Fort Huachuca, Arizona, Contract DA-36-039-AMC-00878(E), 249 pp.

Köhler, Hilding, 1933: Meteorologische Turbulenzuntersuchungen 1, Kungl Svenska Vetenskapsakademiens Handlingar, Tredje Serien, Band 13, No. 1, pp. 1-54.

Kung, Ernest C., 1963: Climatology of Aerodynamic Roughness Parameter and Energy Dissipation in the Planetary Boundary Layer of the Northern Hemisphere, pp. 37-96 in Studies of the Effects of Variations in Boundary Conditions on the Atmospheric Boundary Layer, Annual report from Department of Meteorology, University of Wisconsin to Department of Meteorology, Fort Huachuca, Arizona, Contract DA-36-039-AMC-00878, 149 pp.

Kung, Ernest C., 1966: Kinetic Energy Generation and Dissipation in the Large-Scale Atmospheric Circulation, Monthly Weather Review, Vol. 94, No. 2, pp. 67-82.

Kutzbach, John E., 1961: Investigations of the Modification of Wind Profiles by Artificially Controlled Surface Roughness, pp. 71-113 in Studies of the Three-Dimensional Structure of the Planetary Boundary Layer, Annual report from Department of Meteorology, University of Wisconsin to Department of Meteorology, Fort Huachuca, Arizona, Contract DA-36-039-SC-80282, 170 pp.

Laikhtman, D. L., 1961: Physics of the Boundary Layer of the Atmosphere, translated from Russian by I. Shechtman, Israel

Program for Scientific Translations, Jerusalem 1964, 200 pp. Available from OTS, U. S. Department of Commerce, Washington 25, D. C.

Lettau, H. H., 1939: Atmosphärische Turbulenz. Akademische Verlagsgesellschaft, Leipzig, 283 pp.

Lettau, H., 1950: A Re-examination of the "Leipzig Wind Profile" Considering Some Relations Between Wind and Turbulence in the Frictional Layer, Tellus, Vol. 2, No. 2, pp. 125-129.

Lettau, H. H. and Ben Davidson, 1957: Exploring the Atmosphere's First Mile, Pergaman Press, New York, 578 pp.

Lettau, H. H., 1959: Wind Profile, Surface Stress and Geostrophic Drag Coefficients in the Atmospheric Surface Layer, pp. 241-257 in Atmospheric Diffusion and Air Pollution, Edited by F. N. Frenkiel and P. A. Sheppard (Advances in Geophysics, Vol. 6), Academic Press, New York, 471 pp.

Lettau, H. H., 1961: A Generalized Mathematical Model of the Mean-Velocity Distribution in Fully Turbulent Duct Flow, pp. 115-142 in Studies of the Three-Dimensional Structure of the Planetary Boundary Layer, Annual report from Department of Meteorology, University of Wisconsin to Department of Meteorology, Fort Huachuca, Arizona, Contract DA-36-039-SC-80282, 170 pp.

Lettau, H. H., 1962: Theoretical Wind Spirals in the Boundary Layer of a Barotropic Atmosphere, Beiträge zur Physik der Atmosphäre, Vol. 35, No. 314, pp. 195-212.

Lumley, John L. and Hans A. Panofsky, 1964: The Structure of Atmospheric Turbulence, Vol. XII, Interscience Monographs and

Texts in Physics and Astronomy, John Wiley, New York, 239 pp.

Mapanao, Leo, 1966: On the Wind Distribution with Height in the Hurricane Boundary Layer, unpublished M.S. thesis, University of Hawaii, Department of Geosciences, 37 pp.

Mildner, P., 1932: Über die Reibund in einer speziellen Luftmasse in den untersten Schichten der Atmosphäre, Beiträge zur Physik der freien Atmosphäre, Band 19, pp. 151-158.

Möller, Fritz, 1931: Austausch und Wind, Meteorologische Zeitschrift, Vol. 48, No. 2, pp. 69-80.

Onishi, Gaishi, (1966): personal communication of research to be contained in Final Report of Contract DA-AMC-28-043-64-G2 and issued by Hawaii Institute of Geophysics, University of Hawaii, August 1966.

Orville, Harold D., 1964: On Mountain Upslope Winds, Journal of the Atmospheric Sciences, Vol. 21, No. 6, pp. 622-633.

Panofsky, H. A. and A. A. Townsend, 1964: Change in Terrain Roughness and the Wind Profile, Quarterly Journal of the Royal Meteorological Society, Vol. 90, No. 384, pp. 147-155.

Prandtl, L., 1935: The Mechanics of Viscous Fluids, in Aerodynamic Theory, edited by W. F. Durand, Vol. III, pp. 34-208, J. Springer, Berlin. (Reprinted by Dover, New York, in 1963).

Prandtl, L., and O. G. Tietjens, 1934: Fundamentals of Hydro- and Aeromechanics, reprinted by Dover Publications, Inc., New York in 1957 by special arrangement with the United Engineering Trustee's, Inc., 270 pp.

Priestley, D. H. B., 1959: Turbulent Transfer in the Lower Atmosphere, University of Chicago Press, 130 pp.

Richtmyer, R. D., 1957: Difference Methods for Initial-value Problems, New York: Interscience Publishers, 238 pp.

Rossby, C. G. and R. B. Montgomery, 1935: The Layer of Frictional Influence in Wind and Ocean Currents, Papers in Physical Oceanography and Meteorology MIT and WHOI, Vol. III, No. 3, 101 pp.

Stearns, Charles R. and Heinz H. Lettau, 1963: Report on Two Wind Profile Modification Experiments in Air Flow over the Ice of Lake Mendota, pp. 115-138 in Studies of the Effects of Variations in Boundary Conditions on the Atmospheric Boundary Layer, Annual report from Department of Meteorology, University of Wisconsin to Department of Meteorology, Fort Huachuca, Arizona, Contract DA-36-039-AMC-00878, 149 pp.

Stearns, Charles, 1964: Report on Wind Profile Modification Experiments Using Fields of Christmas Trees on the Ice of Lake Mendota, pp. 59-97 in Studies of the Effects of Variations in Boundary Conditions on the Atmospheric Boundary Layer, Annual report from Department of Meteorology, University of Wisconsin to Department of Meteorology, Fort Huachuca, Arizona, Contract DA-36-039-AMC-00878, 115 pp.

Sutton, O. G., 1951: Atmospheric Turbulence and Diffusion, pp. 492-509 in Compendium of Meteorology, edited by Thomas F. Malone, American Meteorological Society, Boston, 1334 pp.

Sutton, O. G., 1953: <u>Micrometeorology</u>, New York: McGraw-Hill, 333 pp.

Taylor, G. I., 1915: Eddy Motion in the Atmosphere, <u>Philosophical Transactions of the Royal Society, Series A</u>, Vol. CCXV, pp. 1-26.

Taylor, R. J., 1962: Small-scale Advection and the Neutral Wind Profile, <u>Journal of Fluid Mechanics</u>, Vol. 13, pp. 529-539.

Yamamoto, Giichi and Atsushi Shimanuki, 1964: The Determination of Lateral Diffusivity in Diabatic Conditions Near the Ground from Diffusion Experiments, <u>Journal of the Atmospheric Sciences</u>, Vol. 21, No. 2, pp. 187-196.